RSC Advances

REVIEW

View Article Online
View Journal | View Issue

Cite this: *RSC Adv.*, 2019, **9**, 25285

Recent progress in the imaging detection of enzyme activities *in vivo*

Chunjie Yang,[ab] Qian Wang[b] and Wu Ding *[b]

Received 16th June 2019
Accepted 29th July 2019

DOI: 10.1039/c9ra04508b

rsc.li/rsc-advances

Enzymatic activities are important for normal physiological processes and are also critical regulatory mechanisms for many pathologies. Identifying the enzyme activities *in vivo* has considerable importance in disease diagnoses and monitoring of the physiological metabolism. In the past few years, great strides have been made towards the imaging detection of enzyme activity *in vivo* based on optical modality, MRI modality, nuclear modality, photoacoustic modality and multifunctional modality. This review summarizes the latest advances in the imaging detection of enzyme activities *in vivo* reported within the past years, mainly concentrating on the probe design, imaging strategies and demonstration of enzyme activities *in vivo*. This review also highlights the potential challenges and the further directions of this field.

1 Introduction

Enzymes play an important role in many physiological and biological processes, and can serve as critical biomarkers for the pathology of many diseases as abnormal enzyme activities are closely related to the pathology of many diseases.[1–6] Thus, a large number of different methods of measuring the enzyme activity for a range of enzyme families have been developed over the past several decades. The traditional detection methods for performing the enzyme activity analysis mainly include colorimetric assays,[7–10] electrochemical assays[11–13] and luminescence assays.[14–17] Although these technologies for determining enzymatic activities have great value, most researchers are not capable of measuring specific enzyme activity in biological systems in real time, and a non-destructive testing of the activity *in vivo* is still a challenging technical problem.[18] Typically, these technologies are faced with two challenges: avoiding artificial aspects that affect the enzyme activity within the context of the natural biological environment in living subjects and accomplishing the rapid, sensitive and high-resolution detection *in vivo*, particularly, in relatively deep tissues. Recent developments in optical imaging, magnetic resonance imaging (MRI) and nuclear imaging have made it possible to visualize enzyme activities in deep tissues.[19,20] Several pivotal reviews have discussed the advances in enzyme activity detection, with most reviews focusing on specific subcategories, such as small-molecule substrate reporters and protein-based reporters,[21] labelled and unmodified substrates,[22] gold nanoparticle-based biosensors,[23] activatable probes capable of imaging enzyme

[a]College of Health Science, Yuncheng Polytechnic College, Yuncheng, Shanxi 044000, PR China

[b]College of Food Science and Engineering, Northwest A&F University, Yangling, Shaanxi 712100, PR China. E-mail: dingwu10142000@hotmail.com

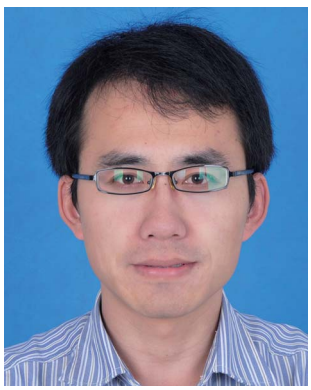

Chunjie Yang received his bachelor's degree in 2009 from Southwest University of Science and Technology. He obtained his master's degree in 2014 from Northwest A&F University. Then, he worked as an assistant at Yuncheng Polytechnic College (from 2014 to 2019). He is now a doctoral candidate at Northwest A&F University under the guidance of Prof. Wu Ding. His current research interests focus on the design and synthesis of fluorescent nanomaterials for bioimaging and detection applications.

Qian Wang received her bachelor's degree and master's degree from Shanxi Agricultural University (2012) and Tianjin Agricultural University (2015), respectively. She is currently studying for a doctor' degree at Northwest A&F University under the guidance of Prof. Wu Ding. Her scientific interests focus on application of luminescent gene luxCDABE in P. aeruginosa biofilm inhibition.

activities,[20] fluorescent probes[24] and methods of measuring enzyme activities *in vivo*.[25] We refer the reader to an earlier review for a more comprehensive coverage of the field.[19] This critical review examined the approaches in the earlier literature towards the *in vivo* imaging of the activity, with an emphasis on the chemical perspective of the probe design, structure and function. Our review is not intended to be a comprehensive discussion of all aspects of enzyme activity detection *in vivo*, but instead, we aim to give a brief summary of the recent advances in this topic. This review summarizes recent advances in enzyme activity detection that have actually been used *in vivo* (*i.e.* that have actually been used in living mice subjects), including optical imaging, MRI, nuclear imaging and photoacoustic imaging-based methods. A systematic discussion is provided on the probe design, imaging strategies and imaging demonstrations of enzyme activities *in vivo*. The potential challenges and the further directions of this field have been discussed as well.

2 Optical modality

Optical modality is a method that detects the photons emitted from bioluminescent or fluorescent contrast agents to generate a two- or three-dimensional image.[19] The optical modality techniques used for enzyme activity detection *in vivo* mainly include fluorescence and bioluminescence imaging.

2.1 Fluorescence imaging

Although a few formal studies have shown that *in vivo* enzyme activities can be evaluated *via* visible fluorescence imaging in mouse models,[26] one of the key limitations, particularly for larger animals (*i.e.* humans), is the limited penetration depth. Thick animal tissue absorbs and scatters photons and generates autofluorescence, all of which obscure an accurate collection and quantification of the signal.[27] The penetration depth of macroscopic fluorescence imaging is limited to only 1–2 mm.[28] Even the high-resolution visible-light optical imaging fails when the subcutaneous tissue depth is greater than 500 microns. As a result, *in vivo* optical imaging has traditionally been limited to endoscopically accessible areas.[29] However, several strategies can overcome these limitations, such as varying the light's wavelength and applying new sophisticated optical approaches (*e.g.*, optical coherence tomography).[30] One of the major reasons that this technology has become feasible is the development of fluorescence probes emitting in the near-infrared (NIR) spectrum where tissues exhibit low absorption.[31] It has been predicted that NIR fluorescent light can penetrate several centimetres,[30,32,33] and possibly even more than ten centimetres.[21] In addition, autofluorescence and light scattering are decreased in the NIR spectrum.[34] In general, NIR imaging probes include two groups: small-molecule probes and nanoparticle (NP)-based probes. A number of approaches have been utilized to improve the activation or targeting of the NIR probes. Often these schemes are based on a quenching–dequenching effect, where in the native state, the probe is quenched and then following a specific molecular structure change with their intended enzyme, it becomes highly fluorescent. In the past years, these techniques have been extensively validated and used in various studies on enzyme activity detection *in vivo* (Table 1). Pre-quenched probes are widely used for imaging enzymes, and they are made up of three components: a fluorophore, a quencher dye and an enzyme-cleavable linker. The initial fluorescence of the fluorophore is quenched due to self-quenching, Förster resonance energy transfer (FRET) or non-radiative energy transfer. When the linker is cleaved by a target enzyme, the quencher is released to limit the quenching effect, resulting in fluorescence upon release.[19,20] For an effective analysis of autotoxin (ATX) activity, Madan *et al.* developed and validated a fluorogenic analog of lysophosphatidylcholine (LPC), which enabled the visualization of ATX activity *in vivo*.[56] This is a typical research for enzyme activity detection based on pre-quenched probes. The probe (AR-2) was designed as an analog of LPC, in which a quencher (IRDyeH QC-1) was linked to a mimic of the choline head group and a fluorescent dye (IRDyeH 800CW) was appended to the sn-1 acyl group (Fig. 1A). The fluorescence of AR-2 was quenched until it was activated by ATX, and this could be directly correlated with ATX activity in mice (Fig. 1B and C). In recent decades, similar works have been done on the detection of various enzyme activities, such as that of cysteine cathepsins,[48] leucine aminopeptidase,[52] nitroreductases[50] and β-glucuronidase.[60]

Besides, diverse fluorescent nanoprobes have proven useful as effective enzyme activity detection tools due to such nanoprobes presenting several advantages over conventional fluorescent probes (*e.g.* longer monitoring ability, higher signal-to-background ratio and higher intensity).[65] Chien *et al.* designed a conjugated peptide polymeric nanoparticle to respond to the MMP enzyme.[37] The preparation of enzyme-responsive nanoparticles is shown in Fig. 1D. Most importantly, the fluorescent aggregates were retained for at least 1 week (Fig. 1E). Similar work related to a transmembrane ectoenzyme (CD38) discrimination was demonstrated by Fumey *et al.*, having generated human CD38-specific nanobodies from immunized llamas.[45] These nanobodies were highly specific for modulating the enzymatic activity of CD38.

Wu Ding is a professor in the college of food science and engineering at Northwest A&F University. He received his PhD in 2005 from Northwest A&F University. Additionally, he did his postdoctoral training at the French National Centre for Scientific Research (2006–2008). His current major scientific interests are analytical bioluminescence and chemiluminescence, and their applications in interdisciplinary fields including public health, food safety, and environmental monitoring.

Recently, some self-assembly-based fluorescent probes for imaging enzyme activities were also developed. Ye *et al.* employed an optimized cyclization reaction to control the self-assembly of a fluorescent molecule, and applied it to image caspase-3/7 activity *in vivo* (Fig. 2A).[58] The probe offered the following advantages: (1) a more-extensive biodistribution, (2) deeper tissue penetration and (3) longer residence time in the target tissue of interest. The same self-assembly strategy may be widely used for the non-invasive imaging of enzyme activities *in vivo*. Moreover, a self-assembled fluorescent nanoprobe was developed for the detection and imaging of legumain.[66] The probe was constructed by Cys(StBu)–Ala–Ala–Asn–Lys(Cy5.5)–CBT, which was first reduced and subjected to a condensation reaction to self-assemble with self-quenched fluorescence by an aggregation-caused quenching (ACQ). The nanoparticles disassembled and the NIR fluorescence was released when the Ala–Ala–Asn peptide substrate was recognized and digested by legumain (Fig. 2B).

Although the emergence of various NIR fluorescence probes has led to significant advances in the field of enzyme activity detection *in vivo*, absolute intensity-dependent NIR fluorescence probes can fail to accurately quantify the enzyme activity due to the fact that the probes may be influenced by target concentration-independent experimental or physiological factors (such as cross-talk between the emission and excitation spectra, weakening the ability to capture valid signals).[67] In response to this challenge, some strategies have been designed and proposed to mitigate the effects of a nonspecific background. Among these methods, one simple way to minimize nonspecific effects is to utilize a ratiometric fluorescence strategy. A detectable ratio signal was obtained from two independent signal fluctuations, avoiding the influence of various confounding factors; therefore, ratiometric fluorescence probes can facilitate more accurate and reliable quantitation. For example, a ratiometric fluorescent probe NH-Glu was developed for the selective sensing of β-glucuronidase (GLU) by Huo and colleagues.[68] The probe was successfully used for the real-time visualization of GLU in zebrafish without the interference of the biological matrix. However, the probe is not very suitable for *in vivo* experiments due to the emission wavelength being in the

Table 1 Summary of the recent published reports on *in vivo* NIR imaging of enzyme activity

Target analyte	Fluorescence donor	Emission wavelength (nm)	Experimental subject	Reference
Matrix metalloproteinases (MMPs)	Cy5.5	695	MDA-MB-435 tumor-bearing mice	35
	Alexa750	830	4T1luc tumors mice	36
	Alexa Fluor 647	670	Tumor-bearing mice	37
	Alexa750	770	Adult male BALB/cByJ mice	38
	Alexa680	700	C57BL/6 mice	39
	Alexa680	700	C57BL/6 mice	40
	Alexa680	700	C57BL/6 mice	41
	Alexa680	700	Tumor-bearing mice	42
	Cy5.5	692	C57BL/6 mice	43
	Alexa680	700	DBA1/J mice, C57Bl6/J mice	44
II transmembrane ecto-enzyme (CD38)	Alexa680	702	Mice	45
Renin	VivoTag-S680	690	C57BL/6 mice	46
Cysteine cathepsin	Cy7	767	Male CD-1 mice	47
	Cy5	700	C57BL/6J mice	48
	Cy5.5	720	Tumor-bearing mice	49
Nitroreductase	HXPI	705	Zebrafish	50
	CytoCy5S	660	Mice	51
Leucine aminopeptidase	Hemicyanine (HC)	705	Mice	52
β-Galactosidase	DCDHF	615/665	Mice	53
	Dicyanomethylene-4*H*-pyran (DCM)	500/685	Mice	54
Thrombin	Cy5	700	Mice	55
Autotaxin (ATX)	IRDyeH800CW	800	Tumor-bearing mice	56
Protease	Alexa680	700	C57BL/6 mice	39
	Alexa750	800	H292 xenograft mouse	57
Cathepsin	Alexa680	693	C57BL/6 mice	39
	Alexa680	700	DBA1/J mice	44
	Cy5.5	670–900	Tumor-bearing mice	58
	Cy5	670	Tumor-bearing mice	59
β-Glucuronidase	Hemicyanine (HC)	718	Mice, zebrafish	60
	IR-820	835	Tumor-bearing mice	61
	4-Hydroxy-1,8-naphthalimide (NH)	445/556	Zebrafish	62
Carboxylesterase	1,3-Dichloro-9,9-dimethyl-9*H*-acridin-2(7)-one (DDAO)	700	Mice	63
Prolyl endopeptidases	HiLyte fluo 647	700	Tumor-bearing mice	64

visible light region. Gu and co-workers developed an enzyme-activatable ratiometric NIR probe (DCM-βgal) for real-time fluorescent β-gal activity quantification.[54] The probe was designed by grafting a β-gal activatable unit onto a DCM-OH moiety. An obvious ratiometric fluorescent signal (I_{685nm}/I_{500nm}) was observed when excited at the isosbestic point of 450 nm (Fig. 3A). The probes share many advantages such as high photostability, large Stokes-shift and pH independence. More importantly, this probe was successfully applied for the *in vivo* imaging of mice bearing subcutaneously implanted tumors. In addition, the *in vivo* real-time capture of β-gal activity with a high-resolution 3D view was performed (Fig. 3B). Subsequently, a similar interesting work was presented by Kim's group, who developed a ratiometric fluorescent probe (DCDHF-βgal) for the *in vivo* visualization of β-gal.[53] In this study, β-gal induced an obvious red-shift from 615 to 665 nm in the emission peaks with maximum intensity of the DCDHF-βgal (Fig. 3C). *In vivo* imaging experiments for ratiometric detection were conducted with an intravenous injection of DCDHF-βgal into mice bearing HepG2 xenograft tumors. The results shown in Fig. 3D suggest that the tumor could be clearly visualized by the *in vivo* fluorescence imaging with an emission at 600–700 nm. All these findings indicated that the ratiometric NIR fluorescent probes could be a promising imaging tool for the quantification of enzyme activity *in vivo*.

However, in most studies, the penetrability of the NIR fluorescent probes was insufficient to detect the enzyme activity in organs deep within the body and imaging can only be done of the subcutaneous tumor of the mouse model. In recent years, several well-designed NIR fluorescent probes have been designed to monitor enzyme activities in deeper tissues, such as the GI tract,[64] intestinal tract[60,63] and liver.[52,61,63] The recognition mechanism and deep tissue images of target enzymes using the special probes are shown in Fig. 4. It is noteworthy that all the probes were activatable and were designed to have fluorescence emission in the near-infrared (NIR) range to guarantee a high tissue-penetration capacity among these five studies (Fig. 4a–e). For example, Jin and co-workers designed an activatable NIR fluorescent probe (HC-glu) for the fluorescent evaluation of endogenous β-glu activity in the intestinal tracts of mice.[60] The

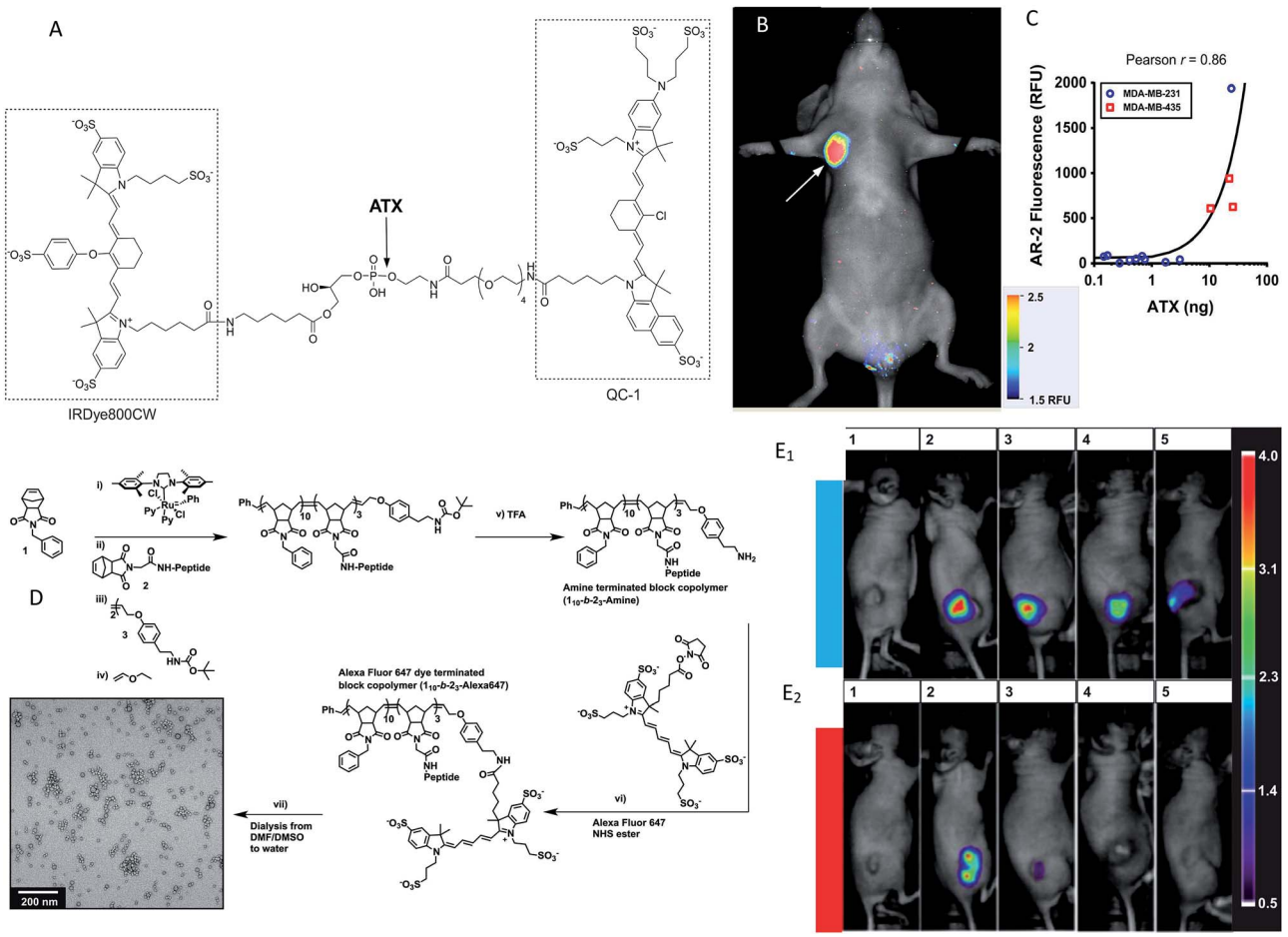

Fig. 1 Fig. 1 (A) Structure of AR-2. (B) Schematic representation of the NIRF imaging of a mouse bearing an MDA-MB-231 tumor (arrow) after being injected with AR-2. (C) There is a significant negative relativity between the tumor fluorescence and ATX. (D) Preparation of enzyme-responsive micellar nanoparticles. (E) Schematic representation of the relative retention levels of enzyme-responsive nanoparticles vs. control particles with HT-1080 tumors. (E1) Nanoparticle M injected. (E2) Nanoparticle MD injected. (A–C) Reproduced from ref. 56. Copy right 2013 Madan et al. D and E) Reproduced from ref. 37. Copy right 2013 American Chemical Society.

probe was designed by grafting a D-glucuronic acid residue onto a hemicyanine skeleton *via* a glycosidic bond (Fig. 4b). The initial maximum intensity of the absorption peak was approximately 670 nm. When HC was released by GLU from the reaction system, a remarkable fluorescence increase was observed at 718 nm (approximately a 40-fold increase). Moreover, a number of commercial NIR fluorescent probes have been developed for enzyme imaging *in vivo*.[38–41,44] In addition, new generations of NIR detectors (fluorescence molecular tomography, FMT) allow the tomographic imaging of enzyme activities with high positional accuracy.[31]

However, the sensitive and selective detection of enzyme activities in deeper tissues by NIR fluorescent probes remains a formidable challenge because of the poor penetration and high scattering. To the best of our knowledge, there have been no successful studies on the non-invasive NIR fluorescent imaging of enzyme activities in deeper tissues. Fluorescence imaging in the NIR-II region (wavelength 1000–1700 nm) may be more desirable over traditional NIR-I imaging owing to its deeper tissue penetration, reduced photon scattering and lower autofluorescence even though it has some problems, such as poor biocompatibility and low fluorescence quantum yields, which limit its application for *in vivo* imaging with enough resolution.[69–71] Over the years, several classes of fluorescent NIR-II probes, such as carbon nanotubes, small molecules, Ag2S dots and polymers, have been developed for NIR-II fluorescence imaging for diversified biomedical applications.[72–75] In general, the use of NIR fluorescent probes for improving the effectiveness of enzyme activity imaging in deeper tissues is only in its infancy, and future years should see an increase in the use of these types of fluorescent probes with newer optical approaches, such as optical coherence tomography (OCT) and diffuse optical tomography.

2.2 Bioluminescence imaging

Bioluminescence generally refers to the emission of light that is generated by the enzymatic reaction of luciferase enzymes and its substrates from a living system.[76] Bioluminescence imaging (BLI) has been broadly used as a powerful platform for *in vivo* animal imaging due to its favorable spectral properties and the lack of toxicity of its substrate.[77] Bioluminescent light can usually be detected at a depth of few centimetres underneath the epidermis, although the exact limit is dependent on the sensitivity of the detector and the intensity of the light.[78] The most widely used BLI method is based on the firefly luciferase (FLuc) and its substrate D-luciferin from *Photinus pyralis*, owing to its maximum emission being in the red and near-infrared wavelengths, making FLuc suitable for *in vivo* imaging. In general, bioluminogenic probes are designed as the "caged luciferin", in which the specific position of luciferin (or aminoluciferin) is caged by some specific functional groups. These caged luciferins do not emit bioluminescence until the luciferins (or aminoluciferins) are generated or released *via* reacting with target enzymes and then oxidized by luciferase.[79] On the basis of this strategy, highly responsive bioluminescent probes as these have been proven to be relatively cheap, animal friendly and to offer much more efficient penetrating power than fluorescence,[80] and hence their use has been well established for many enzymes, such as monoamine oxidase,[81] caspase,[82,83] glutathione *S*-transferase,[81,84] sulfatase,[85] protein kinase,[86] β-galactosidase,[77,87] β-lactamase,[88] CYP450,[89] aminopeptidase N[90] and nitroreductase.[91–93] A typical example was given by Li and

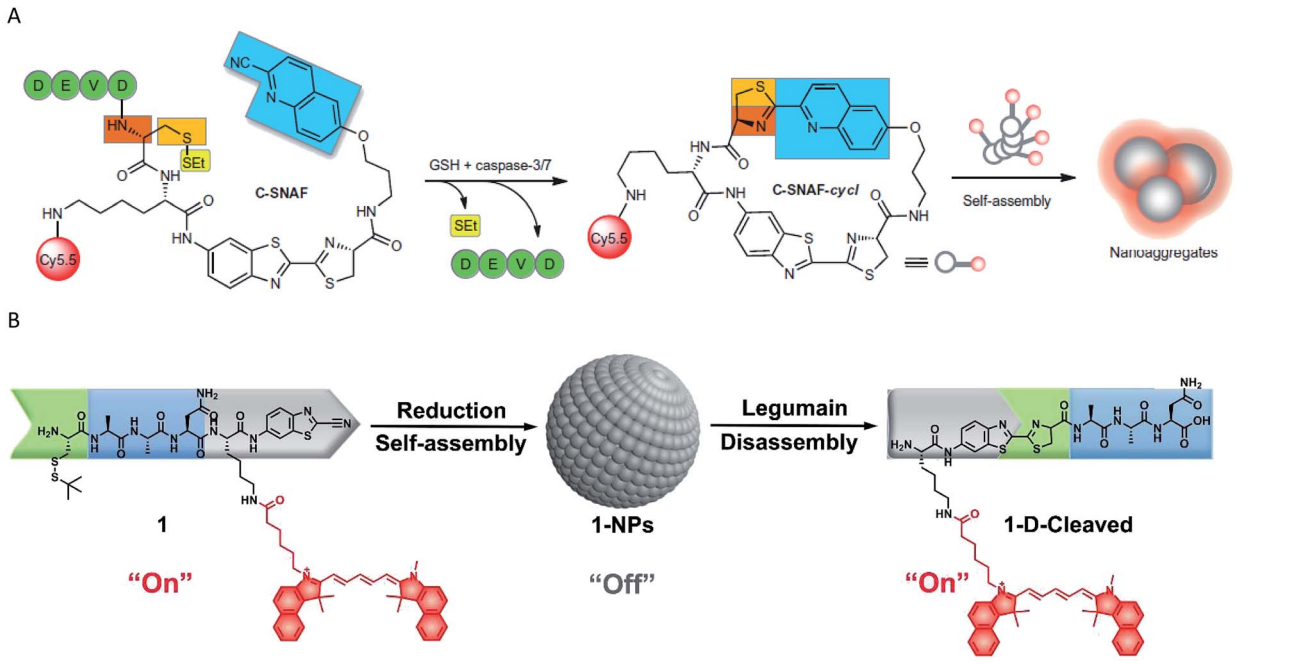

Fig. 2 (A) Schematic representation of the mechanism of *in vivo* imaging by caspase-3/7 activity. Reproduced from ref. 58. Copyright 2014 Springer Nature. (B) Schematic representation of the mechanism of *in vivo* imaging by legumain. Reproduced from ref. 66. Copyright 2018 American Chemical Society.

co-workers, who designed two bioluminogenic probes to detect the aminopeptidase N (APN) activity both *in vitro* and *in vivo via* grafting D-aminoluciferin onto the N-terminus of the APN recognition amino acid(s).[90] In the presence of APN, the probes released free D-aminoluciferin due to the caging groups being removed by the enzymolysis reaction. The released D-aminoluciferin produced a photon *via* reaction with the firefly luciferase (Fig. 5A). Then, the two probes were used for the *in vivo* imaging of APN activity in nude mice. Further imaging analysis in Fig. 5B illustrated that the probes had the capacity to image APN activity *in vivo*. Subsequently, through similar strategies, several research groups have developed bioluminescent probes for the chemoselective visualization of nitroreductase (NTR)[92] and tyrosinase[94] in a tumor model. An excellent work was recently presented by Godinat's group, who demonstrated the *in vivo* applicability of this biocompatible reaction, a new method to visualize and quantify the activity of caspase 3/7 protease.[95] This reaction was between D-cysteine and 6-hydroxy-2-cyanobenzothiazole (OHCBT). First, free D-cysteine was released from the caspase 3/7 peptide substrate (DEVD-(D-Cys)). Then, 6-amino-D-luciferin was formed with the progress of D-cysteine's reaction with 6-amino-2-cyanobenzothiazole (NH_2-CBT). Finally, there was an emission of light that was generated by the enzymatic reaction of 6-amino-D-luciferin and luciferase (Fig. 5C). Importantly, the ratio between the signals produced from the d-GalN/lipopolysaccharide (LPS)-treated group and the control group was statistically significantly higher than that of the commercial substrate (DEVD-aminoluciferin) (Fig. 5D). All these findings showed that this strategy was superior to the commercially available substrate for the imaging of caspase 3/7 activity. Moreover, the split luciferin approach enables signal stability and a modular construction of bioluminescent probes. A further improvement in this approach was carried out by Bittner's group, who presented a general strategy for dual-analyte (H_2O_2 and caspase 8) detection in animals *via* utilizing the *in situ* formation of firefly luciferin from two complementary caged precursors.[82] This strategy constituted an AND-type molecular logic gate. To establish this approach, the probe Peroxy Caged Luciferin-2 (PCL-2) was designed to generate 6-hydroxy-2-cyanobenzothiazole (HCBT) by reacting with H_2O_2. The probe z-Ile-Glu-ThrAsp-D-Cys (IETDC) was designed to release D-cysteine catalyzed by caspase 8. If and only if both chemicals were released, a bioluminescent signal was generated.

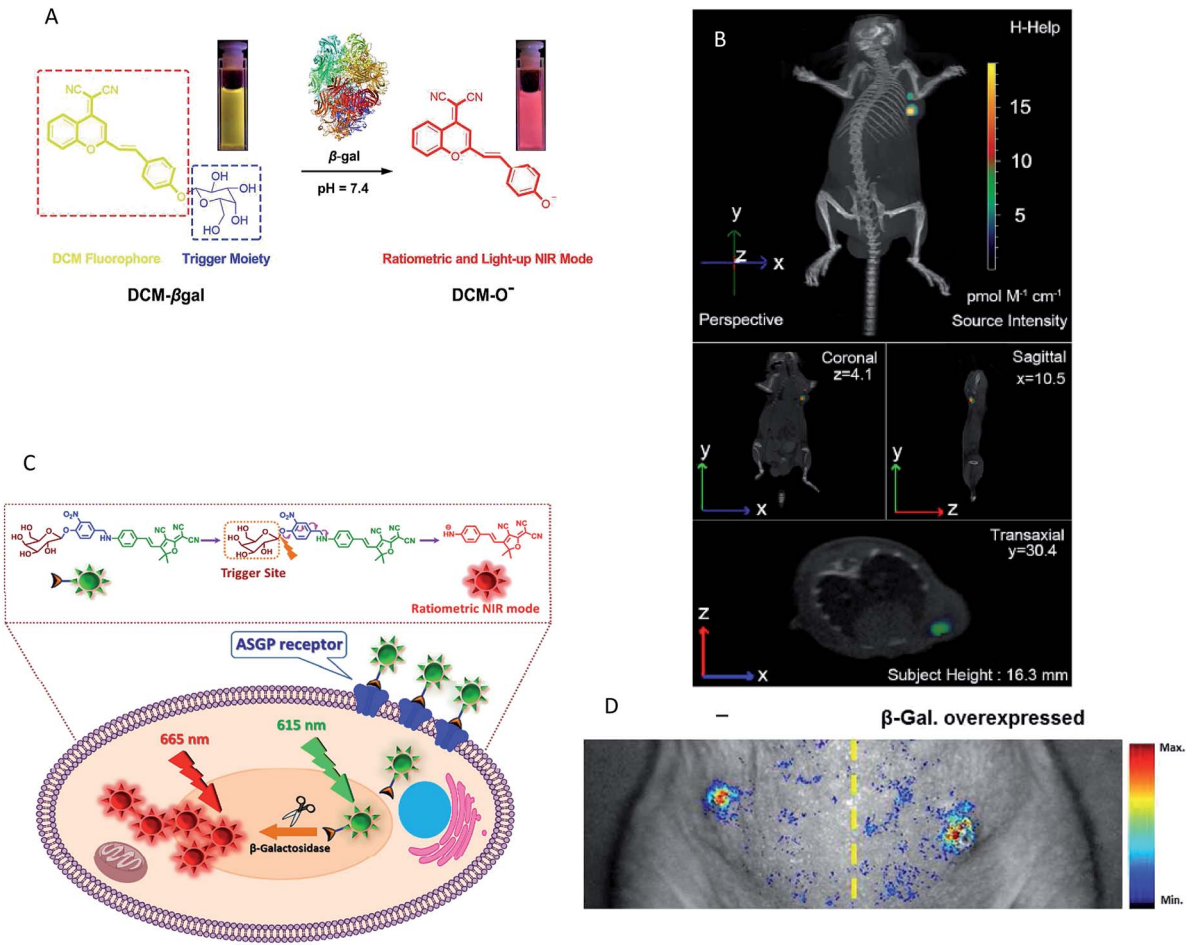

Fig. 3 (A) Conceptual scheme of β-Gal enzymatic activation of DCM-βgal. (B) Three-dimensional *in vivo* imaging of DCM-βgal. (C) Conceptual scheme of DCDHF-βgal when encountering β-Gal and the following fluorescence change. (D) *In vivo* fluorescence imaging of DCDHF-βgal. (A and B) Reproduced from ref. 54. Copyright 2016 American Chemical Society. (C and D) Reproduced from ref. 53. Copyright 2017 Elsevier.

Although great progress has been made over the past decade in the detection of enzyme activities *in vivo* by bioluminescence imaging, there are still many challenges ahead. First, though the enzyme–substrate specificity is crucial, many luciferases are sensitive to their environment, such as pH and reactive oxygen species, which can result in an increase in the number of false positives. Second, although many types of bioluminescence probes have been developed to target enzyme activity, the *in vivo* application of these probes is still unsatisfactory; for instance, the emitted light of all luciferases is inherently weak, and only a fraction of the light typically reaches the detector due to the majority of bioluminescent photons being scattered or absorbed by endogenous chromophores in biological tissues.[78,96] Although these have been largely solved by engineering luciferases to produce near-infrared (NIR) bioluminescent photons, the improvement is often limited because the light intensity reduces with a red-shift in the peak emission.[97] Finally, since the caged luciferins reaction require two co-existing enzymes (luciferase and target enzyme), caged luciferins are normally dedicated to transgenic animals for expressing luciferase.

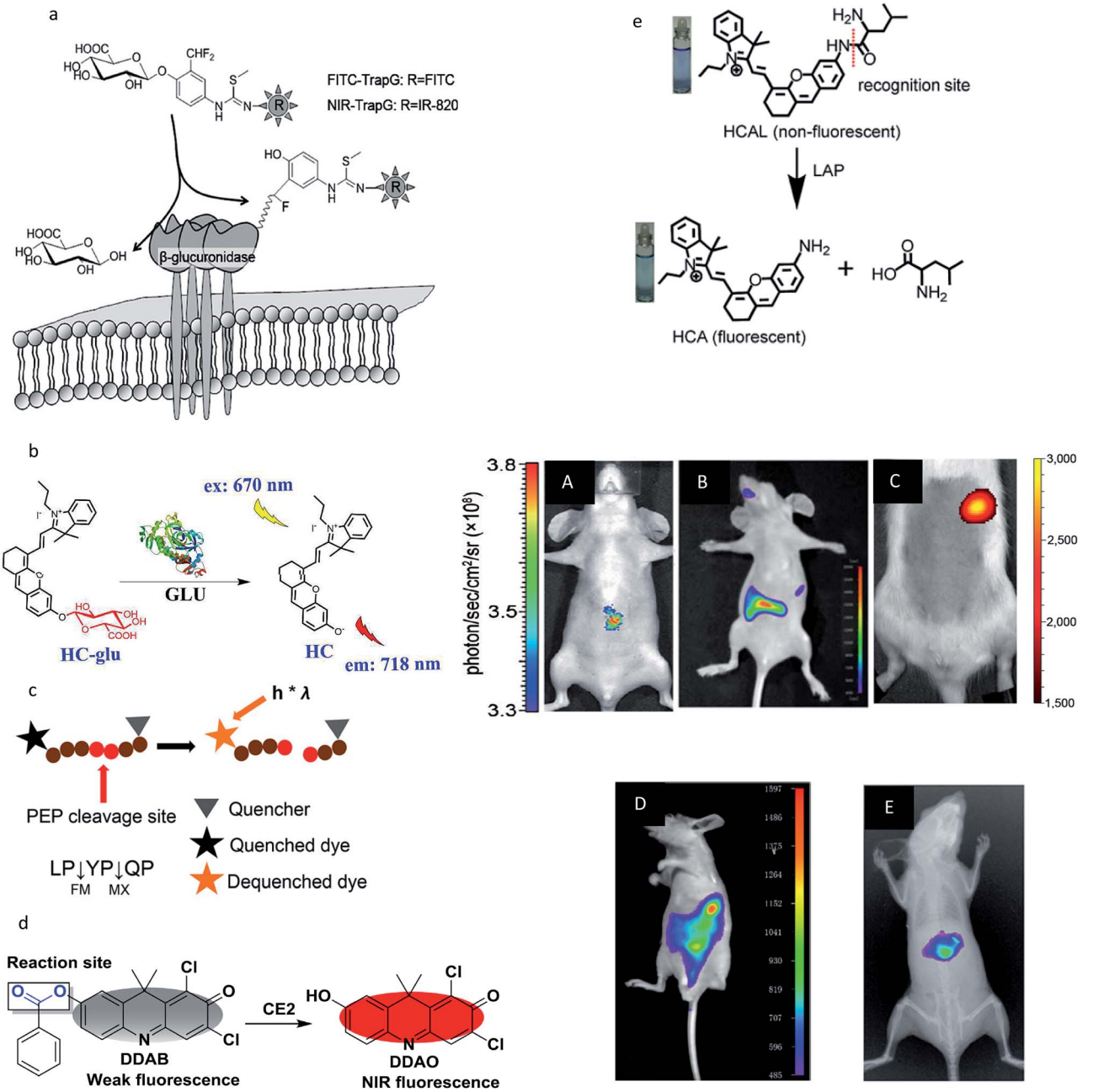

Fig. 4 (a–e) Recognition mechanism of the probes. (A–E) Real-time activity measurement in deep tissues of a mouse. (a and A) Reproduced from ref. 61. Copyright 2012 American Chemical Society. (b and B) Reproduced from ref. 60. Copyright 2018 American Chemical Society. (c and C) Reproduced from ref. 64. Copyright 2011 National Academy of Sciences. (d and D) Reproduced from ref. 63. Copyright 2016 Elsevier. (e and E) Reproduced from ref. 52. Copyright 2017 Royal Society of Chemistry.

Owing to the requirement of genetic modification, this is limited in clinical applications. However, with the continued development of new luciferases and luciferins, these studies will enhance our ability to study enzyme activities in living organisms.

3 MRI modality

Magnetic resonance imaging (MRI) is a noninvasive imaging method that provides physiological and pathological information of living tissues.[98] Although MRI is capable of high spatial resolution and unlimited tissue penetration, the technology generally requires exogenous contrast agents because of its low sensitivity.[99,100] MR contrast agents can be separated into four categories: T_1 agents, T_2 agents, hyperpolarization agents and chemical exchange saturation transfer (CEST) agents.[30,99]

Some effective strategies have been reported to design MR probes for enzyme activity analysis, such as oligomerization of the probe, the disassembly of nanoparticles, modulation of the hydration number, the switching of solubility, relaxivity enhancement *via* macromolecular binding and the unmasking of CEST-active protons.[19] To date, ^{1}H MRI has been broadly used in this area due to its high sensitivity. As a recent example for T_1/T_2 agents, several ^{1}H MR probes have been designed for β-galactosidase activity imaging by Li's group.[101] They designed a series of β-D-galactosides conjugated with various chelators for assessing β-gal activity in solution by ^{1}H-MRI T_1 and T_2 relaxation mapping. However, ^{1}H-MRI often has the disadvantage of a low signal-to-noise ratio because of large background signals,[102] such that most of this type of contrast agents cannot be used for *in vivo* imaging.

For target-specific detection, heteronuclear MRI techniques have attracted more and more attention for alternative methodologies to the ^{1}H-based MR imaging of enzymes. ^{19}F MRI is considered a promising method mainly because ^{19}F has higher selectivity than ^{1}H MRI,[103] and there is no interference from the background signals *in vivo* because fluorine is essentially absent in mammalian tissues. However, unlike the mechanism of ^{1}H-MRI, ^{19}F MRI usually offers ambiguous localization and poor sensitivity[104,105] and few ^{19}F MRI probes can be applied to detect enzymatic activity *in vivo*. Several promising enzyme *in vivo* sensing ^{19}F MRI probes have been reported in the past few years.[106–108] A representative study was reported by Yuan *et al.*, who demonstrated a dual-functional probe for the specific detection of legumain (Lgmn) based on the self-assembly and disassembly of a probe conferring ^{19}F MR signals "off" and "on", respectively.[103] The ^{19}F nanoparticles were constructed by the self-assembly of a ^{19}F probe (1-NPs) upon intracellular glutathione (GSH) reduction. When the nanoparticles were disassembled by Lgmn, the ^{19}F MRI signal was output for Lgmn detection (Fig. 6A). In addition, a control compound probe (2-NPs), whose ^{19}F MRI signal could be turned "off" in cells, was

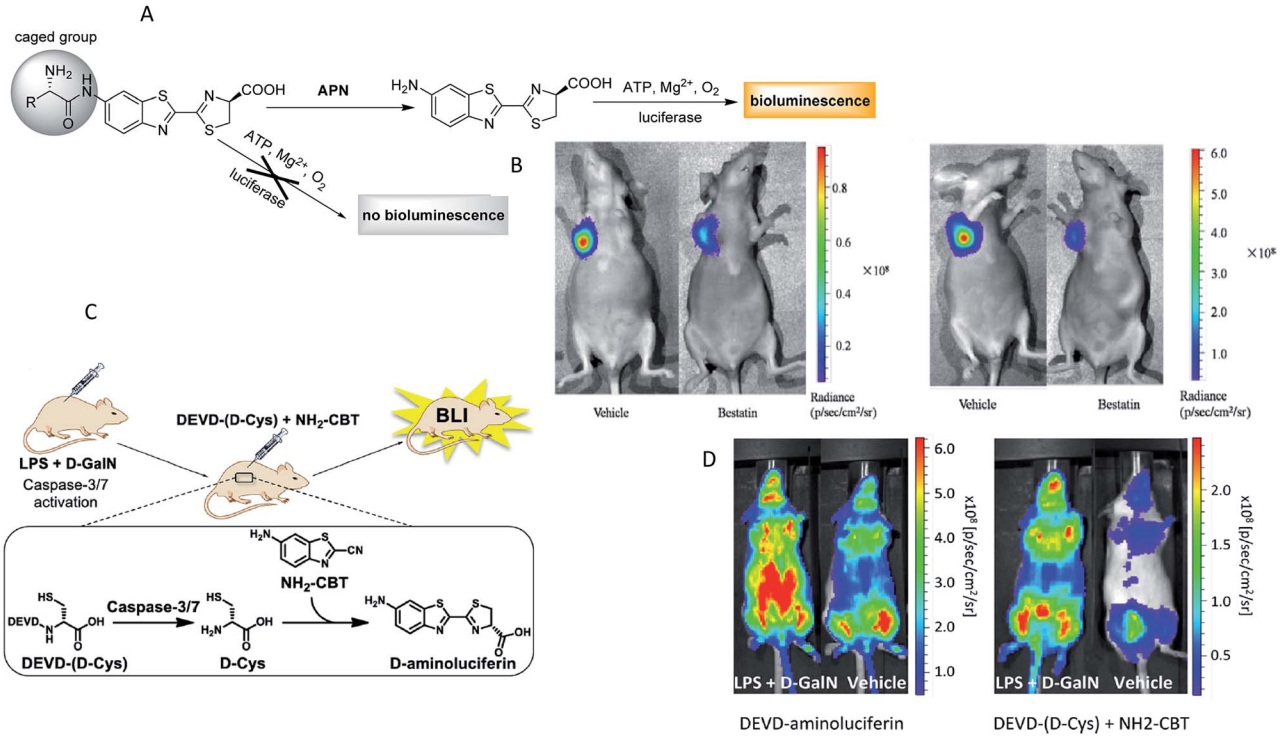

Fig. 5 (A) Schematic of bioluminogenic probes for detecting APN activity. (B) Bioluminescence imaging of APN activity in the implanted ES-2-luc cells for probe 1(left), probe 2(right). (C) Schematic of caspase-3/7 activity imaging with DEVD-(D-Cys) peptide and NH_2-CBT. (D) Representative image of mice treated with LPS and D-GalN or vehicle, injection of DEVD-aminoluciferin or a combination of DEVD-(D-Cys) and NH_2-CBT reagents. (A and B): Reproduced from ref. 90. Copyright 2014 American Chemical Society. (C and D) Reproduced from ref. 95. Copyright 2013 American Chemical Society.

designed and studied. As shown in Fig. 6B, strong ^{19}F MRI signals were detected from (or near) the tumors in zebrafish while healthy zebrafish did not show detectable ^{19}F MRI signal when given an injection of the same dose of 1-NPs. In addition, ^{19}F MRI signals could be detected from the nontumor sites of the tumor-bearing zebrafish and the healthy zebrafish after the injection of large-dose 2-NPs. These results illustrated that the ^{19}F MRI probe 1-NPs could successfully be used to detect Lgmn activities in zebrafish at low doses. Most recently, Akazawa's group reported a similar nanoprobe FLAME-DEVD2 for

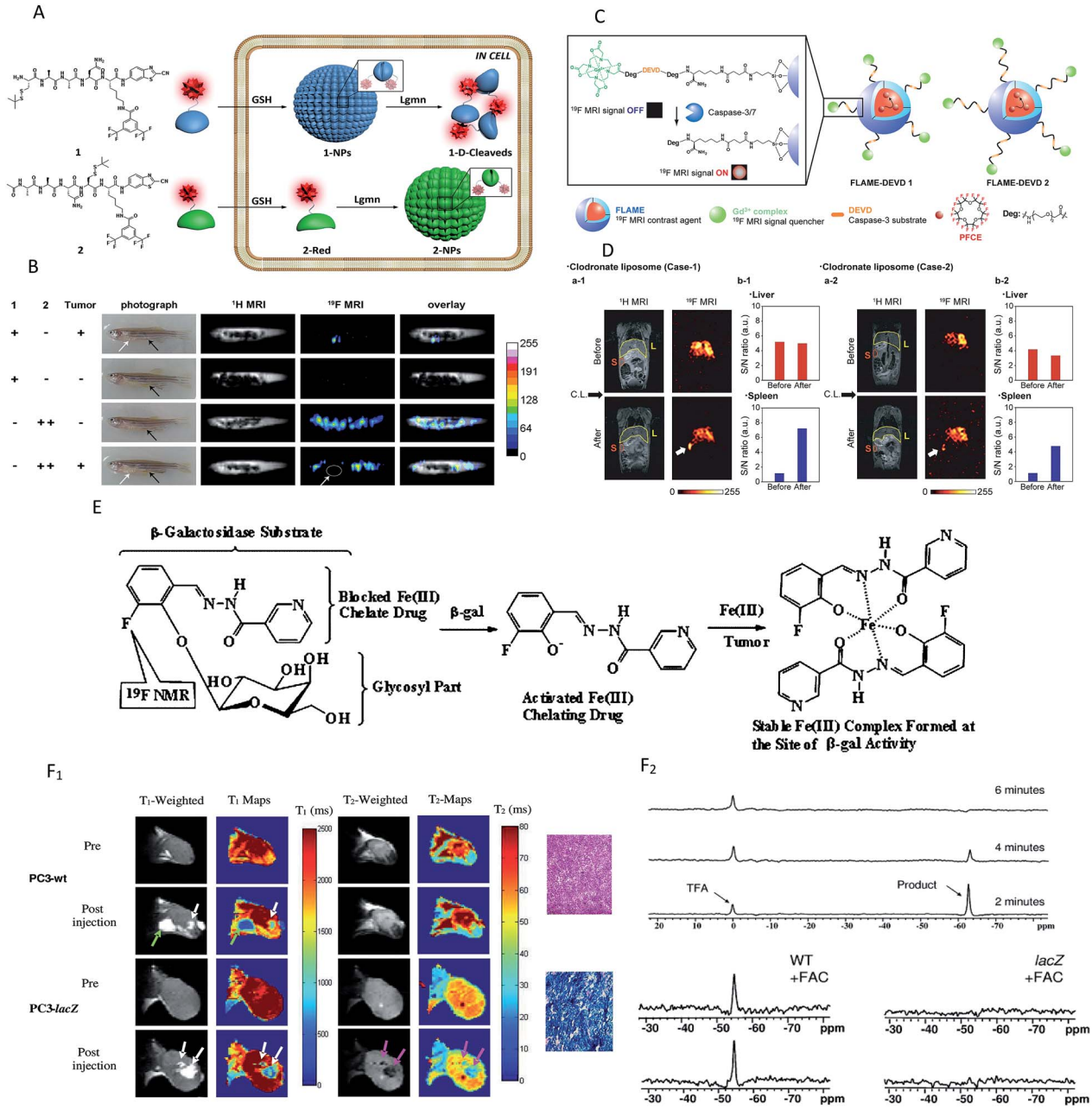

Fig. 6 (A) Schematic illustration of the self-assembly followed by disassembly of 1-NPs, and the self-assembly of 2-NPs. (B) Representative image of tumour-bearing or healthy zebrafish after being injected with the probes. White arrows indicate the tumour sites, and black arrows indicate the injection sites. White circle indicates the tumour location. (C) Schematic of FLAME-DEVD *X* (*X* = 1, 2), enzyme-responsive ^{19}F MRI nanoprobes for detecting caspase-3/7 activity. (D) ^{19}F MRI of caspase-3/7 activity in a mouse. FLAME-DEVD was intravenously injected into a mouse (before). Then, clodronate liposome was intravenously injected (after). L: liver. S: spleen. (E) Schematic of MRI contrast for detecting β-gal activity. (F) F_1: imaging β-gal activity *in vivo* by ^{1}H MRI. Green arrow indicates anomalous injection outside the tumour. White arrows indicate injection inside th tumour. Pink arrows indicate the change in T-weighted images and T_2 values was obvious in the lacZ-transfected tumours post-injection of the agent and FAC. F_2: Detection of β-gal activity *in vivo* by ^{19}F NMR. NaTFA served as a chemical shift reference at 0 ppm and remained quite constant. (A and B) Reproduced from ref. 103. Copyright 2015 American Chemical Society. (C and D) Reproduced from ref. 107. Copyright 2018 American Chemical Society. (E and F) Reproduced from ref. 109. Copyright 2012 American Chemical Society.

detecting caspase-3/7 activity in mice spleen.[107] In this study, a tandemly repeated substrate peptide sequence was incorporated into a ^{19}F MRI signal activation strategy to improve the cleavage efficiency of peptides (Fig. 6C). After the injection of FLAME-DEVD 2 and an apoptosis-inducing reagent, the ^{19}F MRI signals in the spleen were clearly enhanced, and the S/N ratios were 6.2-fold (Case 1) and 4.2-fold (Case 2) higher than before the clodronate liposome (CL) injection (Fig. 6D). These results demonstrate that the nanoprobe FLAME-DEVD2 could successfully be used for activity imaging of caspase-3/7 in the spleen of a living mouse.

The ^{19}F and ^{1}H MRI modalities both have their own advantages and disadvantages. Hence, several dual-function probes for a synergistic combination of ^{1}H and ^{19}F MRI to overcome the restraints of both imaging techniques have been designed to monitor the β-galactosidase activity, in which ^{19}F-MRI recognizes substrate accumulation and conversion, whereas ^{1}H-MRI reveals its location and magnitude.[102,105,109] A typical example was found in the study by Yu and co-workers, who reported a dual-function MRI probe to detect the β-galactosidase activity in human tumor xenografts growing in mice.[109] It is worth noting that the probe was introduced as a fluorine atom into iron chelating aroylhydrazone aglycones of β-D-galactopyranosides (Fig. 6E). When activated by β-gal, the fluoroaroylhydrazones were released and then could be trapped by Fe^{3+} at the site of enzyme activity to form highly relaxing complexes *in situ*. Meanwhile, the complexes caused strong T_2 relaxation, providing clear ^{1}H MRI to reveal β-gal activity. While the agents and ferric ammonium citrate (FAC) were injected into wild-type (WT) (no β-gal expression) and PC3 tumor (β-gal expression) xenografts growing in mice, T_1 and T_2 decreased significantly in lacZ tumors, but not in WT tumors (Fig. 6F$_1$). Besides, no product or substrate ^{19}F NMR signal was detected in the spectrum of lacZ tumors, but the agent was decreased slowly in the WT tumors (Fig. 6F$_2$). In brief, the above results showed that the dual-modality approach can detect both the substrate and product and thus improves the reliability of enzyme detection.

Chemical exchange saturation transfer (CEST) MRI is a relatively new approach that allows the monitoring of protein properties *in vivo*.[110] In this method, the CEST agents can reduce the MRI signal from water by the exchange of protons with bulk water. The CEST spectrum is a plot of the MR signal amplitude of bulk water *versus* a range of saturation frequencies.[111] In the past few years, CEST MRI has been applied to detect the activity of the urokinase plasminogen activator, alkaline phosphatases, sulfatase enzyme, cathepsin, carboxypeptidase, cytosine deaminase, glutamyl transferase, kallikrein and so on.[112–119] These studies, mostly from Pagel's group, utilized different types of diamagnetic or paramagnetic CEST agents to assess enzyme activities. For a typical example, this group detected the *in vivo* enzyme activity of g-glutamyl transferase (GGT) within mouse models using CEST MRI.[118] As shown in Fig. 7A, the agent was synthesized by binding a glutamyl moiety to 4-amino salicylic acid. This agent generated two independent CEST signals, a signal at 4.8 ppm based on the aryl amide moiety and a signal at 9.2 ppm based on the salicylic acid moiety. When the glutamyl moiety of the CEST agent was cleaved by the GGT enzyme, the CEST signal at 4.8 ppm disappeared, whereas the CEST signal at 9.2 ppm remained approximately constant. This result showed that the ratio of the two signals could be used to detect the GGT enzyme activity. Further experiments *in vivo* were performed with mouse models of OVCAR-8 and OVCAR-3 human ovarian cancer as well as muscle, which had high, low, and no GGT activity, respectively. The parametric maps of the % CEST demonstrated high activity in the OVCAR-8 tumor, low activity in the OVCAR-3 tumor, and no activity in the muscle tissue (Fig. 7B). As a consequence, CatalyCEST MRI was shown to be an effective method for detecting GGT enzyme activity within *in vivo* tumor mice models. In a similar way, this group also successfully detected the activity of kallikrein 6 in an *in vivo* tumor model.[119]

Moreover, recent *in vivo* studies have demonstrated that MRI has a strong potential for the non-invasive, selective monitoring of enzymatic activity. However, only a few related studies have been performed in tumor mouse models, and there is hardly any monograph on MR imaging of enzymes activity in human body. The main drawbacks of MRI are represented by the limited sensitivity and potentially toxic effects of its probes. Thus, it is vital to design MRI contrast agents with lower toxicity and higher sensitivity. CEST and hyperpolarized probes appear to be promising potential tools in MR-based enzyme activity imaging applications. In addition, particular attention should

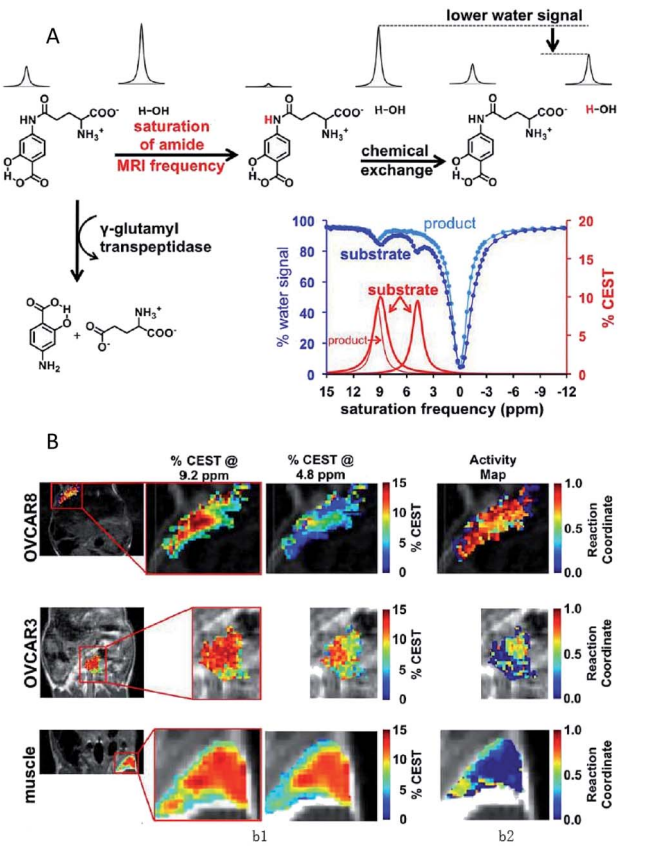

Fig. 7 (A) The CEST-FISP MRI protocol of the agent. (B) CatalyCEST MRI of GGT activity *in vivo*. Reproduced from ref. 118. Copyright 2017 International Society for Magnetic Resonance in Medicine.

be given to design "smart" MRI agents by combining MRI and nanotechnology.[95] However, to achieve this aim, much more basic work should be done and related studies need to be performed.

4 Nuclear modality

Enzyme activity imaging based on nuclear imaging mainly includes positron emission tomography (PET) and single-photon emission computed tomography (SPECT). PET is an imaging technique that relies on the detection of positrons that are produced by the decay of radioactive isotopes.[120,121] The positron has the ability to penetrate the human body, so the probe can always be imaged, regardless of the location of the target.[100,122] The major advantages of PET are its high sensitivity and precision spatial quantitation capabilities. SPECT is a similar technique based on the detection of gamma ray emission from radioactive decay.[123] However, PET normally is an order of magnitude more sensitive than SPECT.[124] The common isotopes that can be incorporated within the radioisotope-based agents mainly include ^{18}F, ^{124}I, ^{123}I, ^{68}Ga and ^{111}In. Over the past years, nuclear imaging has been widely developed for the detection of several enzyme activities, such as β-glu, MMP, histone deacetylases, urokinase plasminogen activator (uPA) and drug metabolizing enzymes.[125–131] Thus, in this section, several representative examples were selected to provide a brief illustration. Chuang and colleagues developed a PET imaging technology for detecting the MMP activity *in vivo*.[126] In this report, the probe was synthesized in three steps: first, a polyethylene glycol (PEG_{5000}) molecule was linked to the N-terminus of a MMP2/9 peptide substrate, then PEG-peptide was attached to a tetramethyl rhodamine group (TMR), and finally ^{18}F was labelled to form the probe (PEGpeptide-^{18}F-TMR). The test mechanism was as follows: first, the hydrophobic ^{18}F-TMR was released by MMP and then preferentially accumulated at the active sites of the protease. Finally, MMP activity *in vivo* was determined through the detection of radioactivity from ^{18}F-TMR by PET (Fig. 8A). As shown in Fig. 8B, radio signals were selectively accumulated in HT1080 tumors but not in MCF-7 tumors when mice bearing HT1080 (MMP-expressing) and MCF-7 tumors (MMP-no expressing) were injected with the same dosage of PEG-peptide-^{18}F-TMR. These results showed that PEG-peptide-^{18}F-TMR was effective for the detection of MMP activity *in vivo*. Using a similar design

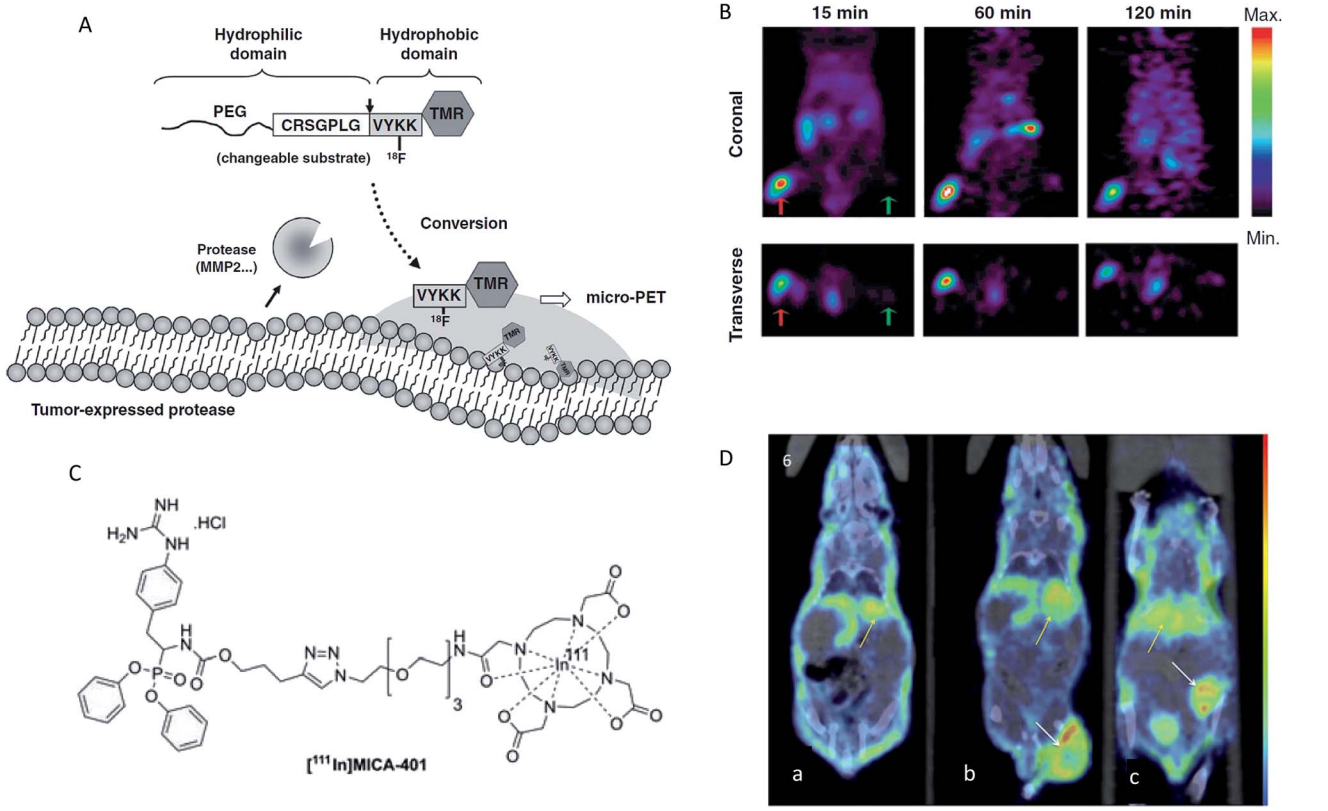

Fig. 8 (A) Schematic representation of the MMP activity-based PET strategy. (B) Micro-PET imaging of MMP activity *in vivo*. Mice bearing established HT1080 (left hind legs) and MCF-7 (right hind legs) tumours were injected with PEG-peptide-^{18}F-TMR. The red arrows indicate HT1080 human fibrosarcomas in left hind legs. The green arrows indicate MCF-7 human breast adenocarcinomas in right legs. (C) Chemical structures of fluor-18 and indium-111 labelled [111In]MICA-401. (D) Representative SPECT images at 95 h post injection of the uPA activity-based probe [111In]MICA-401 in the three models. (a) Healthy control mouse; (b) HT-29 tumour-bearing mouse; (c) MDA-MB-231 tumour-bearing mouse. The white arrows indicate tumours and yellow arrows indicate liver. (A and B) Reproduced from ref. 126. Copyright 2012 American Association for Cancer Research. (C and D) Reproduced from ref. 129. Copyright 2016 John Wiley & Sons, Ltd.

principle, PET imaging was also developed for the assessment of β-Glu activity *in vivo*.[128] In addition, SPECT imaging has proved to be a feasible strategy to evaluate *in vivo* uPA activity.[129] Here, the SPECT probe MICA-401 was appropriate to selectively display uPA activity *in vivo* since it can selectively bind to uPA by a covalent bond (Fig. 8C). *In vivo* SPECT images are shown in Fig. 8D. Both the tumors were easily detectable and a moderate tumor uptake was observed for the HT-29 (uPA-expressing) and MDA-MB-231 (uPA-expressing) models. These results showed that the imaging of uPA activity *in vivo* by SPECT was feasible.

However, nuclear imaging involves radiation exposure, a high cost of entry and high ongoing costs.[132,133] The design of PET and SPECT tracers used for enzymatic target imaging is a challenging task because the agents need to have high specificity and affinity towards the target enzyme.[134] In addition, storage and handling of these radioactive materials also involve a certain level of danger and may result in harmful consequences.[100] Although these disadvantages have limited its broader practical application, it is still a potential technique for the detection of enzyme activities in a large animal model due to the penetration depth of this technique being almost unlimited.

5 Photoacoustic modality

The ultrasonic technique is a major clinical tool for soft-tissue imaging because of its low cost, high penetration depths and easy operation.[135,136] However, ultrasound is limited by its inability to identify all abnormalities in tissues. Photoacoustic imaging (PAI) is able to complement and enhance ultrasound imaging. PAI is based on optical excitation and ultrasonic detection. First, a thermally induced pressure jump is caused by the light absorption of tissues, and then the pressure jump creates and launches ultrasonic waves. Finally, two-dimensional or three-dimensional images are formed by collecting and processing the ultrasonic signal.[137–139] PAI integrates the advantage of the high penetration of ultrasound imaging and the high contrast of optical imaging.[140,141]

In recent years, several studies have successfully shown the potential of PAI for the detection of enzyme activities in *in vivo* applications.[142–149] An interesting study was recently presented by Liu's group, who used an activatable photoacoustic (PA) probe to estimate the distribution of MMP2 cleavage sites inside living tumor tissues.[142] In this probe (GPD), a fluorescent dye molecule Dye680 (absorption peak at ~680 nm) was used to couple with gold nanocages (GNCs) (absorption peak at ~800 nm) *via* a specific enzymatic peptide substrate (SH-PEG-NH_2). As shown in Fig. 9A, the Dye680 were released through the rupture of the peptide substrate by MMP-2. The PA signals changed significantly because of the change in the intrinsic absorption profile caused by the different retention speeds of GNCs and Dye680p. *In vivo* PAI images for MMP 2 activity are shown in Fig. 9B, where it can be seen that strong PA signals appeared immediately at both 680 and 770 nm after injection in a GPD injection group, while no obvious changes at either 680 or 770 nm were observed in a GPD + inhibitor injection group. In other words, the experiment showed that the probe has the ability to estimate the distribution of the protease activity in the tumor periphery region.

In addition, if the excitation light source is far-infrared light or microwaves, the imaging technique (usually called thermoacoustic imaging, TAI) can provide higher penetration than PAI.[140,150] Despite all this, only a few PAI (TAI) examples exist so far for the detection of enzyme activities *in vivo* because the research on exogenous contrast agents is still at the entry level, and most contrast agents have been validated only at a pre-commercial, proof-of-concept stage without approval for clinical use. Much more work will need to be done to improve the PAI probes performance, such as solubility, stability and specific targeting capability.[151] Nevertheless, with the compelling advantages of imaging performance characteristics, such as rivalling the speed of ultrasound imaging, the resolution of MRI and the specificity of nuclear imaging,[152] imaging technologies based on PAI, therefore, are expected to have huge development potential and good application prospects in the detection of enzyme activities *in vivo*.

6 Multifunctional modality

Clearly to date, each method has both advantages and disadvantages. Therefore, the combination of two or more methods may prove more applicable. Multimodality imaging allows the integration of the advantages of a single modality and provides multi-parameter information in a composite imaging

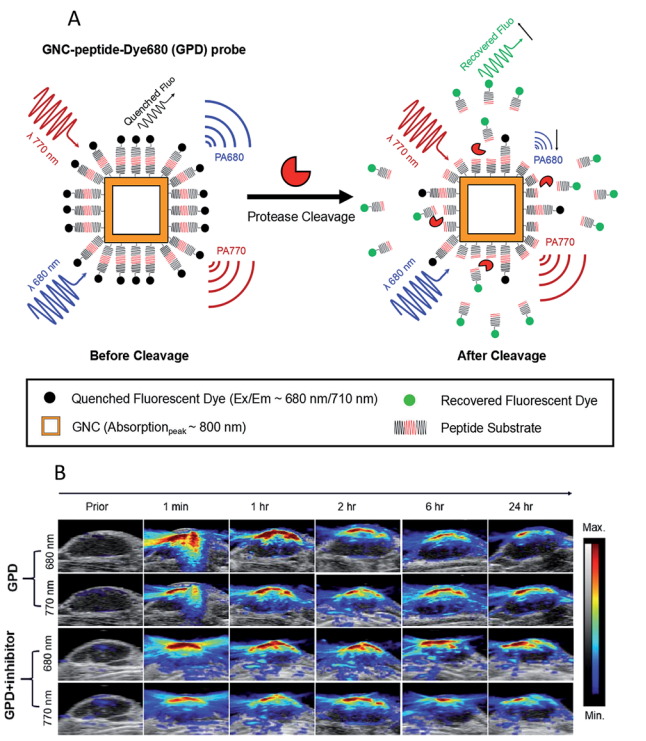

Fig. 9 (A) Schematic design of the activatable probe GPD. The probe is expected to produce a strong PA signal from the GNCs and Dye680, conjugated by a cleavable peptide substrate. (B) PAI after intratumoral injections of GPD probe ± inhibitor. Reproduced from ref. 142. Copyright 2018 World Molecular Imaging Society.

platform,[153] so a growing number of multimodal probes have been designed to clearly delineate the localization and expression of biochemical markers.[154] For the imaging of enzyme activities, the combination of different imaging modalities mainly include NIR-PET imaging,[48,155] NIR-MR imaging,[156] NIR-PA imaging[157] and SPECT/CT.[158,159] A recent significant study described a dual labelled (optical and PET/CT) probe BMV101, which could be used for the imaging of active cathepsins in fibrotic lesions of patients with idiopathic pulmonary fibrosis (IPF).[48] This probe contained a near infrared fluorophore Cy5 for optical imaging and a NOTA chelator for labelling with ^{64}Cu or ^{68}Ga for PET/CT imaging (Fig. 10A).

Optical imaging and PET/CT of cathepsin activity by ^{64}Cu-BMV101 in the bleomycin lung fibrosis model are shown in Fig. 10B and C. The PET-CT signal increased until day 14 and reduced on day 21 in the bleomycin-induced lung fibrosis mice model. In addition, the optical probe signal was consistent with the PET-CT results. These results confirmed that the intensity of signals observed by optical and PET/CT imaging correlated with the levels of cathepsin activity. More importantly, the non-invasive imaging of active cathepsins in human trials was demonstrated for the first time using 68Ga-BMV101 probe (Fig. 10D). In summary, although the overall signal-to-noise ratios were rather poor and more effective probe backbone structures need to be further identified, this research represents significant progress in human trials.

Typically, the multimodality imaging procedure is as follows: the test subject is scanned by different devices, and the images from each device are then overlaid, resulting in a fused image. This may lead to an imprecise co-registration of images and involves a time delay; so, simultaneous measurements by different techniques are critical to the measurement accuracy.[160] Additionally, there are many challenges in the design of multimodal imaging probes, though efforts have been made in this field in recent years.[161,162] Challenges for multimodality imaging probes are summarized nicely in a succinct review

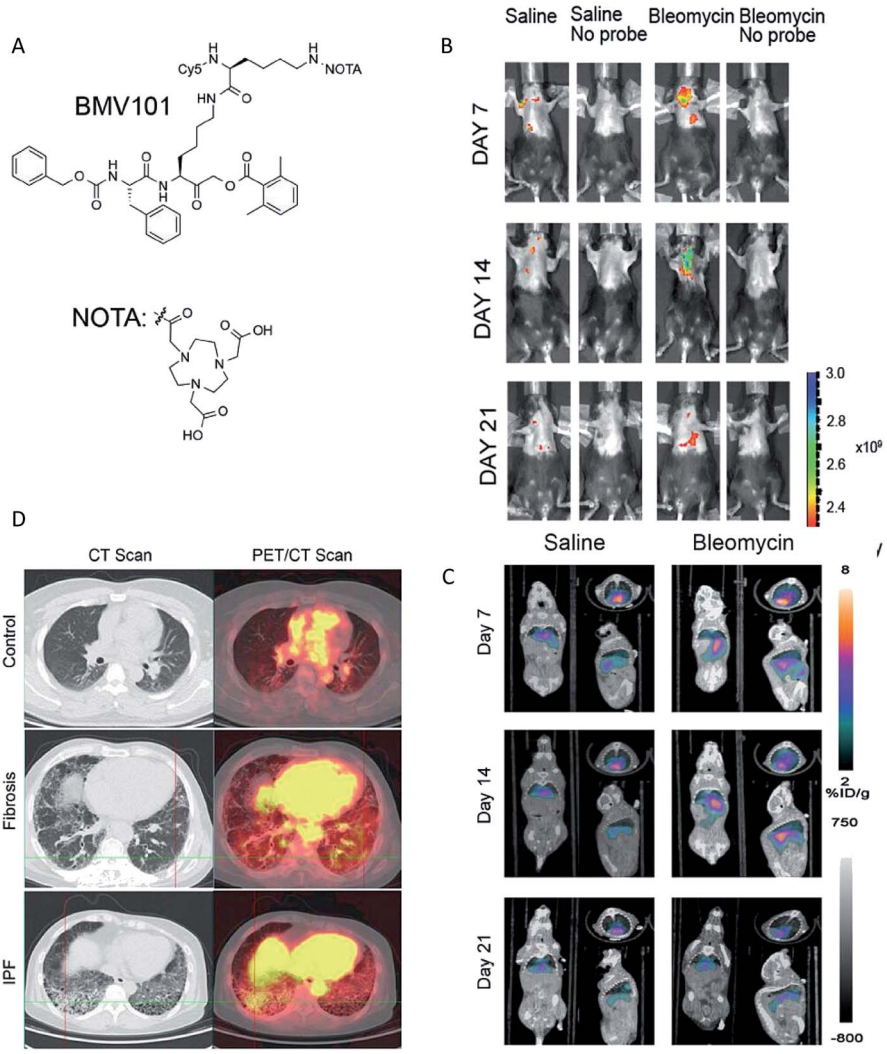

Fig. 10 (A) Structures of the activity based probe BMV101. (B and C) Application of the ^{64}Cu-BMV101 as a dual optical (B)/PET/CT (C) imaging probe. (D) First-in-human application of imaging probe ^{68}Ga-BMV101. Representative scans of patients with idiopathic pulmonary fibrosis (IPF) and unclassifiable pulmonary fibrosis (fibrosis) compared to healthy controls. Reproduced from ref. 48. Copyright 2016 Springer Nature.

published in *Chemical Reviews*,[163] and we refer the reader there for more information. However, in any case, the combination should draw on each other's merits to maximize the synergistic effect rather than choosing imaging modalities at random.

7 Conclusions and outlook

In the past few years, great progress has been made in the detection of enzyme activities *in vivo* based on optical modality, MRI modality, nuclear modality, photoacoustic modality and multifunctional modality. Overall, optical modality is the most thoroughly developed technique, though we anticipate that the other four techniques will all find more important applications in this area. Each imaging modality has its advantages along with limitations. For instance, despite the fact that the NIR optical modality exhibits unique optical properties (*e.g.* relatively low cost, high sensitivity, high biocompatibility and deep penetration) that make it widely used in the imaging of enzyme activities in animal models, the development of alternative strategies of imaging in deeper tissues while retaining a high resolution and signal intensity remains a big challenge. For another example, compared with optical imaging, MR imaging provides deeper tissue penetration, rendering it more appropriate for *in vivo* deep tissue imaging, but MRI provides relatively low sensitivity, and involves a high cost and long imaging time. Therefore, the use of multiple modalities in conjunction seems to be a powerful tool to implement each techniques' advantages, and more effort may be expected in the coming years in this regard. Furthermore, although the imaging of enzyme activity using these technologies has been demonstrated in small animal models, there are still several limitations. First, the type of enzymes that had been detected *in vivo* is far less than *in vitro*. The enzymes currently detected *in vivo* are mainly the hydrolyses used as tumor markers. Further studies should attempt to detect the other classes of enzymes *in vivo*, although it is a challenging task. Second, although some progress has been achieved in the research of the enzyme activity detection *in vivo* over the past few years, more preclinical and clinical trials should be encouraged to ascertain the clinical applicability of these techniques. Additionally, in order to make these technologies more suitable to clinical practice, several characteristics have to be taken into consideration as follows: (1) deep tissue penetration; (2) high sensitivity; (3) high specificity; (4) low toxicity; (5) easy removal and (6) low cost. Finally, advanced imaging equipment, such as multimodal instruments, should be developed for more effective use in *in vivo* applications.

Over recent years, the number of contrast agents for diversified imaging applications is booming significantly. In clinical practice, small-molecule contrast agents are currently prevalent for use in imaging procedures because of their high biocompatibility and favorable excretion pharmacokinetics.[164] However, small molecules cannot be easily multiplexed and cannot be easily designed.[165] In recent decades, the design of various nanomaterial-based contrast agents has played a key role in improving imaging techniques. In general, most nanomaterial-based contrast agents have several promising advantages compared with their small-molecule counterparts, such as high sensitivity, good specificity and multimodal ability.[67] Despite the advantages of using nanomaterial-based contrast agents *in vivo*, the pace of these contrast agents moving into clinical trials remains relatively gradual because of nanomaterial safety concerns. In brief, much work is required in the future to develop more advanced contrast agents for clinical needs.

Furthermore, it is worth noting that another promising area of future development is wireless sensor capsule for *in situ* measuring of biochemical compositions in a large animal or human models.[166–171] This detection scheme using a capsule to bypass the hostile detection environment (*e.g.* deep tissues) offers challenges but potentially provides a new approach for the *in vivo* detection of enzyme activities. We believe that this technology based on optical or electrochemical wireless sensors will become a new trend and have quite high possibilities to become an important research tool, with applications across the detection of enzyme activity in deep tissues, such as in the gastrointestinal tract.

This review summarizes the latest advances in the imaging detection of enzyme activities *in vivo* within the past few years, mainly concentrating on the probe design, imaging strategies and the demonstration of enzyme activity *in vivo*. Although challenges are abound because current approaches are still difficult to achieve the quantitation of enzyme activity in deep tissues with satisfactory results, there is no doubt that the field of detection of enzyme activity *in vivo* will continue to evolve as more innovations in material chemistry, photophysics, biology and clinical medical examinations are achieved.

Conflicts of interest

There are no conflicts to declare.

Acknowledgements

This work was supported by the National Key Research & Development Program, [Grant no. 2016 YFD 0401500, China], Key Disciplines Construction Foundation of the "1331" Project of Shanxi Province (098-091704) and the Fund for Shanxi Key Subject Construction (FSKSC). In addition, special thanks to Prof. Wei Zhao from the School of Food Science and Technology, Jiangnan University, who provided writing advice.

References

1 A. H. Palamakumbura and P. C. Trackman, *Anal. Biochem.*, 2002, **300**, 245–251.
2 R. H. Wijdeven, J. Neefjes and H. Ovaa, *Trends Cell Biol.*, 2014, **24**, 751–760.
3 M. B. Youdim, D. Edmondson and K. F. Tipton, *Nat. Rev. Neurosci.*, 2006, **7**, 295–309.
4 J. Yuan, Y. Q. Xu, N. N. Zhou, R. Wang, X. H. Qian and Y. F. Xu, *RSC Adv.*, 2014, **4**, 56207–56210.
5 G. Leto, N. Gebbia, L. Rausa and F. M. Tumminello, *Anticancer Res.*, 1992, **12**, 235–240.

6 Y. Urano, M. Sakabe, N. Kosaka, M. Ogawa, M. Mitsunaga, D. Asanuma, M. Kamiya, M. R. Young, T. Nagano, P. L. Choyke and H. Kobayashi, *Sci. Transl. Med.*, 2011, **3**, 110–119.
7 J. Wang, L. Wu, J. Ren and X. Qu, *Small*, 2012, **8**, 259–264.
8 X. Xie, W. Xu and X. Liu, *Acc. Chem. Res.*, 2012, **45**, 1511–1520.
9 C. Jiang, C. Yan, J. Jiang and R. Yu, *Anal. Chim. Acta*, 2013, **766**, 88–93.
10 A. Hayat, G. Bulbul and S. Andreescu, *Biosens. Bioelectron.*, 2014, **56**, 334–339.
11 V. Chikkaveeraiah, A. A. Bhirde, N. Y. Morgan, H. S. Eden and X. Chen, *ACS Nano*, 2012, **6**, 6546–6561.
12 L. Wu, J. Wang, L. Feng, J. Ren, W. Wei and X. Qu, *Adv. Mater.*, 2012, **24**, 2447–2452.
13 G. Wang, X. He, G. Xu, L. Chen, Y. Zhu, X. Zhang and L. Wang, *Biosens. Bioelectron.*, 2013, **43**, 125–130.
14 L. J. Kricka, J. C. Voyta and I. Bronstein, *Methods Enzymol.*, 2000, **305**, 370–390.
15 A. Wang, S. Yan, R. Huang, S. Feng, B. Fu, X. Weng and X. Zhou, *Analyst*, 2013, **138**, 2825–2828.
16 H. Ao, Z. Qian, Y. Zhu, M. Zhao, C. Tang, Y. Huang, H. Feng and A. Wang, *Biosens. Bioelectron.*, 2016, **86**, 542–547.
17 Y. Su, S. F. Hickey, S. G. Keyser and M. C. Hammond, *J. Am. Chem. Soc.*, 2016, **138**, 7040–7047.
18 C. H. Tung, U. Mahmood, S. Bredow and R. Weissleder, *Cancer Res.*, 2000, **60**, 4953–4958.
19 A. Razgulin, N. Ma and J. Rao, *Chem. Soc. Rev.*, 2011, **40**, 4186–4216.
20 R. Yan and D. Ye, *Sci. Bull.*, 2016, **61**, 1672–1679.
21 A. Baruch, D. A. Jeffery and M. Bogyo, *Trends Cell Biol.*, 2004, **14**, 29–35.
22 J. P. Goddard and J. L. Reymond, *Trends Biotechnol.*, 2004, **22**, 363–370.
23 E. Hutter and D. Maysinger, *Trends Pharmacol. Sci.*, 2013, **34**, 497–507.
24 T. Wei, F. Wang, Z. Zhang, J. Qiang, J. Lv, T. Chen, J. Li and X. Chen, *Curr. Med. Chem.*, 2018, **25**, 1–33.
25 Y. Ou, R. E. Wilson and S. G. Weber, *Annu. Rev. Anal. Chem.*, 2018, **11**, 509–533.
26 M. Chen, K. W. Cheng, Y. J. Chen, C. H. Wang, T. C. Cheng, K. C. Chang, A. P. Kao and K. H. Chuang, *Sci. Rep.*, 2017, **7**, 3142.
27 W. F. Cheong, S. A. Prahl and A. J. Welch, *IEEE J. Quantum Electron.*, 1990, **26**, 2166–2185.
28 M. Yang, E. Baranov, P. Jiang, F. X. Sun, X. M. Li, L. Li, S. Hasegawa, M. Bouvet, M. Al-Tuwaijri, T. Chishima, H. Shimada, A. R. Moossa, S. Penman and R. M. Hoffman, *Proc. Natl. Acad. Sci. U. S. A.*, 2000, **97**, 1206–1211.
29 A. H. Gandjbakhche, V. Chernomordik, D. Hattery and M. Hassan, *Technol. Cancer Res. Treat.*, 2003, **2**, 537.
30 B. R. Smith and S. S. Gambhir, *Chem. Rev.*, 2017, **117**, 901–986.
31 V. Ntziachristos, C. Bremer and R. Weissleder, *Eur. J. Radiol.*, 2003, **13**, 195–208.
32 N. Won, S. Jeong, K. Kim, J. Kwag, J. Park, S. G. Kim and S. Kim, *Mol. Imaging*, 2012, **11**, 338–352.
33 V. Ntziachristos, J. Ripoll and R. Weissleder, *Opt. Lett.*, 2002, **27**, 333–335.
34 S. A. Hilderbrand and R. Weissleder, *Curr. Opin. Chem. Biol.*, 2010, **14**, 71–79.
35 L. Zhu, F. Zhang, Y. Ma, G. Liu, K. Kim, X. Fang, S. Lee and X. Chen, *Mol. Pharm.*, 2011, **8**, 2331–2338.
36 M. Solomon, K. Guo, G. P. Sudlow, M. Y. Berezin, W. B. Edwards, S. Achilefu and W. J. Akers, *J. Biomed. Opt.*, 2011, **16**, 066019.
37 M. P. Chien, A. S. Carlini, D. Hu, C. V. Barback, A. M. Rush, D. J. Hall, G. Orr and N. C. Gianneschi, *J. Am. Chem. Soc.*, 2013, **135**, 18710–18713.
38 T. Fukui, E. Tenborg, J. H. Yik and D. R. Haudenschild, *Biochem. Biophys. Res. Commun.*, 2015, **460**, 741–746.
39 P. B. Satkunananthan, M. J. Anderson, N. M. De Jesus, D. R. Haudenschild, C. M. Ripplinger and B. A. Christiansen, *Osteoarthritis Cartilage*, 2014, **22**, 1461–1469.
40 J. Schwenck, C. M. Griessinger, K. Fuchs, D. Bukala, N. Bauer, M. Eichner, M. Rocken, B. J. Pichler and M. Kneilling, *Mol. Imaging*, 2014, **13**, 7290.
41 J. Schwenck, F. C. Maier, M. Kneilling, S. Wiehr and K. Fuchs, *J. Visualized Exp.*, 2017, e55180.
42 R. A. Sheth, A. Kunin, L. Stangenberg, M. Sinnamon, K. E. Hung, R. Kucherlapati and U. J. M. I. Mahmood, *Mol. Imaging*, 2012, **11**, 417–425.
43 A. K. Steingraber, S. Schelhaas, A. Faust, A. H. Jacobs, M. Schafers and T. Goerge, *Exp. Dermatol.*, 2013, **22**, 730–735.
44 E. A. Vermeij, M. I. Koenders, A. B. Blom, O. J. Arntz, M. B. Bennink, V. D. B. Wb, P. L. van Lent and V. D. L. Fa, *Mol. Imaging*, 2014, **13**, 1–10.
45 W. Fumey, J. Koenigsdorf, V. Kunick, S. Menzel, K. Schutze, M. Unger, L. Schriewer, F. Haag, G. Adam, A. Oberle, M. Binder, R. Fliegert, A. Guse, Y. J. Zhao, H. Cheung Lee, F. Malavasi, F. Goldbaum, R. van Hegelsom, C. Stortelers, P. Bannas and F. Koch-Nolte, *Sci. Rep.*, 2017, **7**, 14289.
46 J. Zhang, D. V. Preda, K. O. Vasquez, J. Morin, J. Delaney, B. Bao, M. D. Percival, D. Xu, D. McKay, M. Klimas, B. Bednar, C. Sur, D. Z. Gao, K. Madden, W. Yared, M. Rajopadhye and J. D. Peterson, *Am. J. Physiol.*, 2012, **303**, 593–603.
47 D. Caglic, A. Globisch, M. Kindermann, N. H. Lim, V. Jeske, H. P. Juretschke, E. Bartnik, K. U. Weithmann, H. Nagase, B. Turk and K. U. Wendt, *Bioorg. Med. Chem.*, 2011, **19**, 1055–1061.
48 N. P. Withana, X. Ma, H. M. Mcguire, M. Verdoes, W. A. V. D. Linden, L. O. Ofori, R. Zhang, H. Li, L. E. Sanman, K. Wei, S. Yao, P. Wu, F. Li, H. Huang, Z. Xu, P. J. Wolters, G. D. Rosen, H. R. Collard, Z. Zhu, Z. Cheng and M. Bogyo, *Sci. Rep.*, 2016, **6**, 19755.
49 Y. Zhao, Z. Hai, H. Wang, L. Su and G. Liang, *Anal. Chem.*, 2018, **90**, 8732–8735.
50 Z. Li, X. He, Z. Wang, R. Yang, W. Shi and H. Ma, *Biosens. Bioelectron.*, 2015, **63**, 112–116.

51 S. Bhaumik, T. V. Sekar, J. Depuy, J. Klimash and R. Paulmurugan, *Gene Ther.*, 2012, **19**, 295–302.
52 X. He, L. Li, Y. Fang, W. Shi, X. Li and H. Ma, *Chem. Sci.*, 2017, **8**, 3479–3483.
53 E. J. Kim, R. Kumar, A. Sharma, B. Yoon, H. M. Kim, H. Lee, K. S. Hong and J. S. Kim, *Biomaterials*, 2017, **122**, 83–90.
54 K. Gu, Y. Xu, H. Li, Z. Guo, S. Zhu, S. Zhu, P. Shi, T. D. James, H. Tian and W. H. Zhu, *J. Am. Chem. Soc.*, 2016, **138**, 5334–5340.
55 E. S. Olson, M. A. Whitney, B. Friedman, T. A. Aguilera, J. L. Crisp, F. M. Baik, T. Jiang, S. M. Baird, S. Tsimikas, R. Y. Tsien and Q. T. Nguyen, *Integr. Biol.*, 2012, **4**, 595–605.
56 D. Madan, C. G. Ferguson, W. Y. Lee, G. D. Prestwich and C. A. Testa, *PLoS One*, 2013, **8**, e79065.
57 K. R. Wong, E. Menendez, C. S. Craik, W. M. Kavanaugh and O. Vasiljeva, *Biochimie*, 2016, **122**, 62–67.
58 D. Ye, A. J. Shuhendler, L. Cui, L. Tong, S. S. Tee, G. Tikhomirov, D. W. Felsher and J. Rao, *Nat. Chem.*, 2014, **6**, 519–526.
59 M. Verdoes, K. Oresic Bender, E. Segal, W. A. van der Linden, S. Syed, N. P. Withana, L. E. Sanman and M. Bogyo, *J. Am. Chem. Soc.*, 2013, **135**, 14726–14730.
60 Y. Jin, X. Tian, L. Jin, Y. Cui, T. Liu, Z. Yu, X. Huo, J. N. Cui, C. P. Sun, C. Wang, J. Ning, B. Zhang, L. Feng and X. Ma, *Anal. Chem.*, 2018, **90**, 3276–3283.
61 T. C. Cheng, S. R. Roffler, S. C. Tzou, K. H. Chuang, Y. C. Su, C. H. Chuang, C. H. Kao, C. S. Chen, H. I-Hong, K. Y. Liu, L. T. Cheng and Y. L. Leu, *J. Am. Chem. Soc.*, 2012, **134**, 3103–3110.
62 X. Huo, X. Tian, Y. Li, L. Feng, Y. Cui, C. Wang, J. Cui, C. Sun, K. Liu and X. Ma, *Sens. Actuators, B*, 2018, **262**, 508–515.
63 Q. Jin, L. Feng, D. D. Wang, J. J. Wu, J. Hou, Z. R. Dai, S. G. Sun, J. Y. Wang, G. B. Ge, J. N. Cui and L. Yang, *Biosens. Bioelectron.*, 2016, **83**, 193–199.
64 G. Fuhrmann and J. C. Leroux, *Proc. Natl. Acad. Sci. U. S. A.*, 2011, **108**, 9032–9037.
65 H. Lee and Y. P. J. B. R. Kim, *BMB Rep.*, 2015, **48**, 313–318.
66 Y. Zhao, Z. Hai, H. Wang, L. Su and G. Liang, *Anal. Chem.*, 2018, **90**, 8732–8735.
67 X. Huang, J. Song, B. C. Yung, X. Huang, Y. Xiong and X. Chen, *Chem. Soc. Rev.*, 2018, **47**, 2873–2920.
68 X. Huo, X. Tian, Y. Li, L. Feng, Y. Cui, C. Wang, J. Cui, C. Sun, K. Y. Liu and X. Ma, *Sens. Actuators, B*, 2018, **262**, 508–515.
69 A. M. Smith, M. C. Mancini and S. Nie, *Nat. Nanotechnol.*, 2009, **4**, 710–711.
70 S. Diao, G. Hong, A. L. Antaris, J. L. Blackburn, K. Cheng, Z. Cheng and H. Dai, *Nano Res.*, 2015, **8**, 3027–3034.
71 Y. Fan and F. Zhang, *Adv. Opt. Mater.*, 2019, **7**, 1801417.
72 Y. Sun, F. Ding, Z. Zhou, C. Li, M. Pu, Y. Xu, Y. Zhan, X. Lu, H. Li, G. Yang, Y. Sun and P. J. Stang, *Proc. Natl. Acad. Sci. U. S. A.*, 2019, **116**, 1968–1973.
73 F. Ding, Z. Chen, W. Y. Kim, A. Sharma, C. Li, Q. Ouyang, H. Zhu, G. Yang, Y. Sun and J. S. Kim, *Chem. Sci.*, 2019, **10**, 7023–7028.
74 F. Ding, C. Li, Y. Xu, J. Li, H. Li, G. Yang and Y. Sun, *Adv. Healthcare Mater.*, 2018, **7**, e1800973.
75 F. Ding, Y. Zhan, X. Lu and Y. Sun, *Chem. Sci.*, 2018, **9**, 4370–4380.
76 S. Wu, E. Chang and Z. Cheng, *Curr. Org. Synth.*, 2011, **8**, 488–497.
77 T. S. Wehrman, G. V. Degenfeld, P. O. Krutzik, G. P. Nolan and H. M. Blau, *Nat. Methods*, 2006, **3**, 295–301.
78 M. A. Paley and J. A. Prescher, *MedChemComm*, 2014, **5**, 255–267.
79 T. Zhang, L. Du and M. Li, *Chin. Chem. Lett.*, 2015, **26**, 919–921.
80 D. A. Dart and C. L. Bevan, *Methods Mol. Biol.*, 2016, **1443**, 203.
81 W. Zhou, M. P. Valley, J. Shultz, E. M. Hawkins, L. Bernad, T. Good, D. Good, T. L. Riss, D. H. Klaubert and K. V. Wood, *J. Am. Chem. Soc.*, 2006, **128**, 3122–3123.
82 G. C. Van de Bittner, C. R. Bertozzi and C. J. Chang, *J. Am. Chem. Soc.*, 2013, **135**, 1783–1795.
83 E. Adamová, M. Lišková, E. Matalová and K. Klepárník, *Anal. Bioanal. Chem.*, 2014, **406**, 5389–5394.
84 W. Zhou, J. W. Shultz, N. Murphy, E. M. Hawkins, L. Bernad, T. Good, L. Moothart, S. Frackman, D. H. Klaubert, R. F. Bulleit and K. V. Wood, *Chem. Commun.*, 2006, **38**, 4620–4622.
85 J. S. Rush, K. E. Beatty and C. R. Bertozzi, *ChemBioChem*, 2010, **11**, 2096–2099.
86 J. Ø. Moskaug, H. Carlsen and R. Blomhoff, *Mol. Imaging*, 2015, **7**, 35–41.
87 R. Geiger, E. Schneider, K. Wallenfels and W. Miska, *Biol. Chem. Hoppe-Seyler*, 1992, **373**, 1187–1191.
88 H. Yao, M. K. So and J. Rao, *Angew. Chem., Int. Ed.*, 2010, **46**, 7161–7164.
89 Y. Gao, Y. Lin, T. Liu, H. Chen, X. Yang, C. Tian, L. Du and M. Li, *Anal. Chem.*, 2017, **89**, 12488–12493.
90 J. Li, L. Chen, W. Wu, W. Zhang, Z. Ma, Y. Cheng, L. Du and M. Li, *Anal. Chem.*, 2014, **86**, 2747–2751.
91 R. H. Wong, T. Kwong, K. H. Yau and H. Y. Au-Yeung, *Chem. Commun.*, 2015, **51**, 4440–4442.
92 P. Feng, H. Zhang, Q. Deng, W. Liu, L. Yang, G. Li, G. Chen, L. Du, B. Ke and M. Li, *Anal. Chem.*, 2016, **88**, 5610–5614.
93 A. G. Vorobyeva, M. Stanton, A. Godinat, K. B. Lund, G. G. Karateev, K. P. Francis, E. Allen, J. G. Gelovani, E. McCormack, M. Tangney and E. A. Dubikovskaya, *PLoS One*, 2015, **10**, e0131037.
94 S. Li, R. Hu, S. Wang, X. Guo, Y. Zeng, Y. Li and G. Yang, *Anal. Chem.*, 2018, **90**, 9296–9300.
95 A. l. Godinat, H. M. Park, S. C. Miller, K. Cheng, D. Hanahan, L. E. Sanman, M. Bogyo, A. Yu, G. F. Nikitin and A. J. Stahl, *ACS Chem. Biol.*, 2013, **8**, 987–999.
96 A. M. Loening, A. M. Wu and S. S. Gambhir, *Nat. Methods*, 2007, **4**, 641–643.
97 S. T. Adams Jr and S. C. Miller, *Curr. Opin. Chem. Biol.*, 2014, **21**, 112–120.
98 M. A. Hahn, A. K. Singh, P. Sharma, S. C. Brown and B. M. Moudgil, *Anal. Bioanal. Chem.*, 2011, **399**, 3–27.

99 E. Terreno, D. D. Castelli, A. Viale and S. Aime, *Chem. Rev.*, 2010, **110**, 3019–3042.
100 M. Carril, *J. Mater. Chem. B*, 2017, **5**, 4332–4347.
101 X. Li, Z. Zhang, Z. Yu, J. Magnusson and J. X. Yu, *Mol. Pharm.*, 2013, **10**, 1360–1367.
102 J. X. Yu, V. D. Kodibagkar, L. Liu, Z. Zhang, J. Magnusson and Y. Liu, *Chem. Sci.*, 2013, **4**, 2132–2142.
103 Y. Yuan, S. Ge, H. Sun, X. Dong, H. Zhao, L. An, J. Zhang, J. Wang, B. Hu and G. Liang, *ACS Nano*, 2015, **9**, 5117–5124.
104 H. Matsushita, S. Mizukami, Y. Mori, F. Sugihara, M. Shirakawa, Y. Yoshioka and K. Kikuchi, *ChemBioChem*, 2012, **13**, 1579–1583.
105 A. Keliris, I. Mamedov, G. E. Hagberg, N. K. Logothetis, K. Scheffler and J. Engelmann, *Contrast Media Mol. Imaging*, 2012, **7**, 478–483.
106 Y. Yuan, H. Sun, S. Ge, M. Wang, H. Zhao, L. Wang, A. Linna, J. Zhang, H. Zhang, B. Hu, J. Wang and G. Liang, *ACS Nano*, 2015, **9**, 761–768.
107 K. Akazawa, F. Sugihara, T. Nakamura, S. Mizukami and K. Kikuchi, *Bioconjugate Chem.*, 2018, **29**, 1720–1728.
108 M. Kazuya, K. Rui, M. Keigo, I. Hirohiko, T. Yuki, N. Michiko, M. Tetsuya, T. Yousuke and H. Itaru, *Chem.–Eur. J.*, 2013, **19**, 12875–12883.
109 J. X. Yu, V. D. Kodibagkar, R. R. Hallac, L. Liu and R. P. Mason, *Bioconjugate Chem.*, 2012, **23**, 596–603.
110 G. Liu, Y. Liang, A. Bar-Shir, K. W. Chan, C. S. Galpoththawela, S. M. Bernard, T. Tse, N. N. Yadav, P. Walczak, M. T. McMahon, J. W. M. Bulte, P. C. M. van Zijl and A. A. Gilad, *J. Am. Chem. Soc.*, 2011, **133**, 16326–16329.
111 B. Yoo and M. D. Pagel, *J. Am. Chem. Soc.*, 2006, **128**, 14032–14033.
112 G. Liu, Y. Liang, A. Bar-Shir, K. W. Chan, C. S. Galpoththawela, S. M. Bernard, T. Tse, N. N. Yadav, P. Walczak, M. T. McMahon, J. W. Bulte, P. C. van Zijl and A. A. Gilad, *J. Am. Chem. Soc.*, 2011, **133**, 16326–16329.
113 M. Haris, A. Singh, I. Mohammed, R. Ittyerah, K. Nath, R. P. Nanga, C. Debrosse, F. Kogan, K. Cai, H. Poptani, D. Reddy, H. Hariharan and R. Reddy, *Sci. Rep.*, 2014, **4**, 6081.
114 Y. Jamin, T. R. Eykyn, E. Poon, C. J. Springer and S. P. Robinson, *Mol. Imaging Biol.*, 2014, **16**, 152–157.
115 B. Yoo, V. R. Sheth, C. M. Howison, M. J. Douglas, C. T. Pineda, E. A. Maine, A. F. Baker and M. D. Pagel, *Magn. Reson. Med.*, 2014, **71**, 1221–1230.
116 I. Daryaei, M. M. Ghaffari, K. M. Jones and M. D. Pagel, *ACS Sens.*, 2016, **1**, 857–861.
117 S. Sinharay, G. Fernandez-Cuervo, J. P. Acfalle and M. D. Pagel, *Chem.–Eur. J.*, 2016, **22**, 6491–6495.
118 S. Sinharay, E. A. Randtke, K. M. Jones, C. M. Howison, S. K. Chambers, H. Kobayashi and M. D. Pagel, *Magn. Reson. Med.*, 2017, **77**, 2005–2014.
119 S. Sinharay, E. A. Randtke, C. M. Howison, N. A. Ignatenko and M. D. Pagel, *Mol. Imaging Biol.*, 2018, **20**, 240–248.
120 T. F. Massoud and S. S. Gambhir, *Genes Dev.*, 2003, **17**, 545–580.
121 A. Sundin, U. Garske and H. Orlefors, *Best Pract. Res., Clin. Endocrinol. Metab.*, 2007, **21**, 69–85.
122 A. Rahmim, J. Qi and V. Sossi, *Med. Phys.*, 2013, **40**, 064301.
123 M. T. Madsen, *J. Nucl. Med.*, 2007, **48**, 661–673.
124 A. Rahmim and H. Zaidi, *Nucl. Med. Commun.*, 2008, **29**, 193–207.
125 I. F. Antunes, H. J. Haisma, P. H. Elsinga, J. W. Sijbesma, A. Waarde, A. T. Willemsen, R. A. Dierckx and E. F. de Vries, *Nucl. Med. Biol.*, 2012, **39**, 854–863.
126 C. H. Chuang, K. H. Chuang, H. E. Wang, S. R. Roffler, J. T. Shiea, S. C. Tzou, T. C. Cheng, C. H. Kao, S. Y. Wu, W. L. Tseng, C. M. Cheng, M. F. Hou, J. M. Wang and T. L. Cheng, *Clin. Cancer Res.*, 2012, **18**, 238–247.
127 J. Ides, D. Thomae, L. Wyffels, C. Vangestel, J. Messagie, J. Joossens, F. Lardon, P. Van der Veken, K. Augustyns, S. Stroobants and S. Staelens, *Nucl. Med. Biol.*, 2014, **41**, 477–487.
128 Y. C. Su, T. C. Cheng, Y. L. Leu, S. R. Roffler, J. Y. Wang, C. H. Chuang, C. H. Kao, K. C. Chen, H. E. Wang and T. L. Cheng, *Mol. Cancer Ther.*, 2014, **13**, 2852–2863.
129 C. Vangestel, D. Thomae, J. Van Soom, J. Ides, L. Wyffels, P. Pauwels, S. Stroobants, P. Van der Veken, V. Magdolen, J. Joossens, K. Augustyns and S. Staelens, *Contrast Media Mol. Imaging*, 2016, **11**, 448–458.
130 N. Fukumitsu, S. H. Yeh, L. G. Flores Ii, U. Mukhopadhyay, D. Young, K. Ogawa, H. J. Jeong, W. Tong and J. G. Gelovani, *Contrast Media Mol. Imaging*, 2018, **3**, e3612027.
131 A. Mizutani, M. Kobayashi, K. I. Fujita, K. Takahashi, T. Hokama, H. Takasu, K. Nishi, R. Nishii, N. Shikano, K. Fukuchi and K. Kawai, *Nucl. Med. Commun.*, 2018, **39**, 825–833.
132 T. M. Bateman, *J. Nucl. Cardiol.*, 2012, **19**, 3–11.
133 M. Ali, B. Pulli and J. W. Chen, *Curr. Cardiovasc. Imaging Rep.*, 2014, **7**, 9258.
134 B. P. Rempel, E. W. Price and C. P. Phenix, *Mol. Imaging*, 2017, **16**, 1–30.
135 S. Unnikrishnan and A. L. Klibanov, *AJR, Am. J. Roentgenol.*, 2012, **199**, 292–299.
136 F. Kiessling, S. Fokong, P. Koczera, W. Lederle and T. Lammers, *J. Nucl. Med.*, 2012, **53**, 345–348.
137 J. L. Su, B. Wang, K. E. Wilson, C. L. Bayer, Y. S. Chen, S. Kim, K. A. Homan and S. Y. Emelianov, *Expert Opin. Med. Diagn.*, 2010, **4**, 497–510.
138 S. Wang, J. Lin, T. Wang, X. Chen and P. Huang, *Theranostics*, 2016, **6**, 2394–2413.
139 Q. Miao and K. Pu, *Bioconjugate Chem.*, 2016, **27**, 2808–2823.
140 D. Wu, L. Huang, M. S. Jiang and H. Jiang, *Int. J. Mol. Sci.*, 2014, **15**, 23616–23639.
141 L. V. Wang and S. Hu, *Science*, 2012, **335**, 1458–1462.
142 C. Liu, S. Li, Y. Gu, H. Xiong, W. T. Wong and L. Sun, *Mol. Imaging Biol.*, 2018, **20**, 919–929.
143 H. Qin, Y. Zhao, J. Zhang, X. Pan, S. Yang and D. Xing, *Biol. Med.*, 2016, **12**, 1765–1774.
144 L. L. Li, Q. Zeng, W. J. Liu, X. F. Hu, Y. Li, J. Pan, D. Wan and H. Wang, *ACS Appl. Mater. Interfaces*, 2016, **8**, 17936–17943.

145 D. Zhang, G. B. Qi, Y. X. Zhao, S. L. Qiao, C. Yang and H. Wang, *Adv. Mater.*, 2015, **27**, 6125–6130.
146 K. Yang, L. Zhu, L. Nie, X. Sun, L. Cheng, C. Wu, G. Niu, X. Chen and Z. Liu, *Theranostics*, 2014, **4**, 134–141.
147 J. Levi, S. R. Kothapalli, S. Bohndiek, J. K. Yoon, A. Dragulescu-Andrasi, C. Nielsen, A. Tisma, S. Bodapati, G. Gowrishankar, X. Yan, C. Chan, D. Starcevic and S. S. Gambhir, *Clin. Cancer Res.*, 2013, **19**, 1494–1502.
148 A. Dragulescu-Andrasi, S. R. Kothapalli, G. A. Tikhomirov, J. Rao and S. S. Gambhir, *J. Am. Chem. Soc.*, 2013, **135**, 11015–11022.
149 C. Liu, Y. Yang, Z. Qiu, Y. Huang and L. Sun, *Ultrasonics Symposium* IEEE, 2015.
150 W. Ding, Z. Ji and D. Xing, *Appl. Phys. Lett.*, 2017, **110**, e183701.
151 J. Weber, P. C. Beard and S. E. Bohndiek, *Nat. Methods*, 2016, **13**, 639–650.
152 D. Razansky, N. C Deliolanis, C. Vinegoni and V. Ntziachristos, *Curr. Pharm. Biotechnol.*, 2012, **13**, 504–522.
153 D. E. Lee, H. Koo, I. C. Sun, J. H. Ryu, K. Kim and I. C. Kwon, *Chem. Soc. Rev.*, 2012, **41**, 2656–2672.
154 Y. Sun, X. Zeng, Y. Xiao, C. Liu, H. Zhu, H. Zhou, Z. Chen, F. Xu, J. Wang, M. Zhu, J. Wu, M. Tian, H. Zhang, Z. Deng, Z. Cheng and X. Hong, *Chem. Sci.*, 2018, **9**, 2092–2097.
155 H. Lee, W. J. Akers, P. P. Cheney, W. B. Edwards, K. Liang, J. P. Culver and S. Achilefu, *J. Biomed. Opt.*, 2009, **14**, e040507.
156 L. Josephson, M. F. Kircher, U. Mahmood, Y. Tang and R. Weissleder, *Bioconjugate Chem.*, 2002, **13**, 554–560.
157 X. Xia, M. Yang, L. K. Oetjen, Y. Zhang, Q. Li, J. Chen and Y. Xia, *Nanoscale*, 2011, **3**, 950–953.
158 M. Razavian, S. Tavakoli, J. Zhang, L. Nie, L. W. Dobrucki, A. J. Sinusas, A. Michael, R. Simon and M. M. Sadeghi, *J. Nucl. Med.*, 2011, **52**, 1795–1802.
159 M. Razavian, J. Zhang, L. Nie, S. Tavakoli, N. Razavian, L. W. Dobrucki, A. J. Sinusas, D. S. Edwards, M. Azure and M. M. Sadeghi, *J. Nucl. Med.*, 2010, **51**, 1107–1115.
160 Z. Brady, M. L. Taylor, M. Haynes, M. Whitaker, A. Mullen, L. Clews, M. Partridge, R. J. Hicks and J. V. Trapp, *Australas. Phys. Eng. Sci. Med.*, 2008, **31**, 90–109.
161 Y. Xu, M. Tian, H. Zhang, Y. Xiao, X. Hong and Y. Sun, *Chin. Chem. Lett.*, 2018, **29**, 1093–1097.
162 F. Ding, S. Chen, W. Zhang, Y. Tu and Y. Sun, *Bioorg. Med. Chem.*, 2017, **25**, 5179–5184.
163 A. Louie, *Chem. Rev.*, 2010, **110**, 3146–3195.
164 L. Tu, Y. Xu, Q. Ouyang, X. Li and Y. Sun, *Chin. Chem. Lett.*, 2019, DOI: 10.1016/j.cclet.2019.05.022.
165 F. Ding, Y. Fan, Y. Sun and F. Zhang, *Adv. Healthcare Mater.*, 2019, e1900260.
166 K. Kalantar-Zadeh, C. K. Yao, K. J. Berean, N. Ha, J. Z. Ou, S. A. Ward, N. Pillai, J. Hill, J. J. Cottrell, F. R. Dunshea, C. McSweeney, J. G. Muir and P. R. Gibson, *Gastroenterology*, 2016, **150**, 37–39.
167 M. Mimee, P. Nadeau, A. Hayward, S. Carim, S. Flanagan, L. Jerger, J. Collins, S. McDonnell, R. Swartwout, R. J. Citorik, V. Bulovic, R. Langer, G. Traverso, A. P. Chandrakasan and T. K. Lu, *Science*, 2018, **360**, 915–918.
168 K. Kalantar-Zadeh, K. J. Berean, N. Ha, A. F. Chrimes, K. Xu, D. Grando, J. Z. Ou, N. Pillai, J. L. Campbell, R. Brkljača, K. M. Taylor, R. E. Burgell, C. K. Yao, S. A. Ward, C. S. McSweeney, J. G. Muir and P. R. Gibson, *Nat. Electron.*, 2018, **1**, 79–87.
169 J. Z. Ou, J. J. Cottrell, N. Ha, N. Pillai, C. K. Yao, K. J. Berean, S. A. Ward, D. Grando, J. G. Muir, C. J. Harrison, U. Wijesiriwardana, F. R. Dunshea, P. R. Gibson and K. Kalantar-Zadeh, *Sci. Rep.*, 2016, **6**, e33387.
170 P. J. van der Schaar, J. F. Dijksman, H. Broekhuizen-de Gast, J. Shimizu, N. van Lelyveld, H. Zou, V. Iordanov, C. Wanke and P. D. Siersema, *Gastrointest. Endosc.*, 2013, **78**, 520–528.
171 C. Steiger, A. Abramson, P. Nadeau, A. P. Chandrakasan, R. Langer and G. Traverso, *Nat. Rev. Mater.*, 2019, **4**, 83–98.